CrossMark

RESEARCH PAPER

A novel displacement constrained optimization approach for black and white structural topology designs under multiple load cases

Jian Hua Rong[1,2] · Liaohong Yu[1,3] · Xuan Pei Rong[1,2] · Zhi Jun Zhao[2,4]

Abstract The gray problem of displacement constrained topology volume minimization under multiple load cases still is an opening topic of research. A series of topologies with clear profiles generated from an optimization process are very beneficial to method engineering applications. In this paper, a novel displacement constrained optimization approach for black and white structural topology designs under multiple load cases, is proposed to obtain a series of topologies with clear profiles. Firstly, a distribution feature of constraint displacement derivatives is investigated. Secondly, an adaptive adjusting approach of design variable bounds is proposed, and an improved approximate model with varied constraint limits and a volume penalty objective function are constructed. Thirdly, an improved density-based optimization method is proposed for the displacement constrained topology volume minimization under multiple load cases. Finally, several examples are given to demonstrate that the results obtained by the proposed method provide a series of topologies with clear profiles during an optimization process. It is concluded from examples that the proposed method is effective and robust for generating an optimal topology.

1 Introduction

Now, the SIMP (Solid Isotropic Material with Penalty) method is a well-known major topology optimization method (Sigmund and Maute 2013, Deaton and Grandhi 2014). One of its major difficulties is the presence of intermediate densities or gray-scale material in density-based structural topology optimization. Black-and-white solutions are often sought, that is, one (such as Sigmund 2007) expects that the final design includes either elements with full material or no material, excluding gray areas. In past works, researchers usually ensured continuous design variables to be forced toward a black and white solution by applying the SIMP model or the Rational Approximation for Material Properties (RAMP) model and their variants (Sigmund and Maute 2013, Deaton and Grandhi 2014). These models are prone to lead to the checkerboard, the mesh dependence and one-point hinge connection problems (Fujii and Kikuchi 2000, Deaton and Grandhi 2014). Some restriction methods, such as the perimeter method (see Haber 1996), the local gradient method (see, e.g. Petersson and Sigmund 1998) and mesh in-dependency filters (see, e.g. Sigmund and Peterson 1998 and etc.) were proposed to deal with these problems.

But gray bands could thus appear around the topological boundary again. Then, Heaviside projections (Guest et al. 2004; Xia et al. 2012 and etc.) were proposed to deal with

✉ Jian Hua Rong
Rongjhua@aliyun.com

1 School of Automotive and Mechanical Engineering, Changsha University of Science and Technology, Changsha, Hunan Province 410114, People's Republic of China

2 Key Laboratory of Lightweight and Reliability Technology for Engineering Vehicle, College of Hunan Province, Changsha 410114, China

3 School of Physical Science and Technology, Yichun University, Yichun, Jiangxi Province 336000, People's Republic of China

4 Department of Civil Engineering, Changsha University, Changsha, Hunan Province 410003, People's Republic of China

the aforementioned problems. Another method is to employ a specified threshold value to obtain elements with normalized densities equivalent to either 1.0 or 0.0 (see, e.g. Kikuchi et al. 1998). However, it is not evident how to choose the threshold value appropriately in these works.

In the SIMP method, Olhoff et al. (1991) proposed a two-stage approach in which initially the intermediate densities are largely suppressed, with a second-stage design procedure generating the desired solid/empty solution. To achieve the solid/empty target in density-based optimization, Fuchs et al. (2005) introduced a new constraint that is labeled the sum of the reciprocal variables (SRV). Based on the work of Zhou and Rozvany (1991), Guedes and Taylor (1997), and Rietz (2001), Bruns (2005) introduced a penalty into the volume constraint, which does result in more predominantly black-and-white solutions. Groenwold and Etman (2009) developed a simple heuristic approach for the gray-scale suppression. Wood and Groenwold (2010) showed that the non-convex topology problem resulting from the application of the SIMP-like volumetric penalization can be solved by adopting the Falk dual. A method combining a separable constraint and a post-processor based on the sequential linear integer programming was proposed by Werme (2008). In addition to the above methods, other methods include the methods with filtering techniques based on image processing (Sigmund 2007, Wang and Wang 2005), a method based on a complex-shaped beam element and graph-based optimization (Sauter et al. 2008), and hybrid methods combining simulated annealing and SIMP (Garcia-Lopez et al. 2011), or standardized elements (Jang et al. 2009).

To the best of our knowledge, the gray problem of displacement constrained topology volume minimization under multiple load cases still is an opening topic of research. Moreover, a series of topologies with clear profiles can not be obtained by the aforementioned density-based methods during an optimization process. The goal of this paper is to develop a new density-based optimization method in an approximate binary fashion of density variables, and provide a different procedure obtaining an optimal topology, so that it can be adopted to easily obtain a predominantly black-and-white optimal topology and a series of topologies with clear profiles during an optimization process.

Recently, by introducing a series of varied constraint limits, a new structural topological optimization method with displacement constraints, was proposed by Rong and Yi (2010), Rong et al. (2011). However, the scheme of the varied constraint limits can not guarantee that the feasible domain of an approximate optimization model at each later iteration step of an optimization process, was completely coincided with the feasible domain of the original model. And because reciprocal topology variables, which may vary between 1.0 and 10,000.0, were selected as design variables in the method, there still

existed a lot of elements with topology variables between 0.15 and 0.001 in each topology obtained during an optimization process. Then, a strategy was adopted to heuristically remove these elements with small topology variable values.

Although the displacement constrained optimization problem is related with stiffness optimization problems to a large extent, the stiffness optimal design is not the same as the optimal displacement design. The stiffness optimization increases the structural overall stiffness and thus the displacements are roughly reduced as an indirect effect. Despite vast researches on stiffness optimization, the displacement constrained continuum topology optimization is found in relatively less literature (see, Liang et al. 2001, Yin and Yang 2001, Huang and Xie 2010, Liu et al. 2011, Zuo et al. 2012, Zuo and Xie 2014, Deng and Suresh 2015). A basic feature during the process of obtaining a series of topologies with clear profiles, is that the topology variables of only a few of elements are allowed to change within a large range at each iteration step. However, a lot of simulations demonstrate that Lagrange multipliers of the conventional approximate SIMP model (Yin and Yang 2001) all are zeros at the many beginning steps in this kind change fashion of design variables (i.e., relative density variables), if the maximum design domain filled with solid material is selected as its initial design. At this case, design variable changes of the conventional approximate model are not affected by the static equations at the many beginning iteration steps because of the Karush-Kuhn-Tucker (KKT) condition action (Nocedal and Wright 1999). Therefore, in view of the fact, the displacement constrained optimization problem basically is different from the maximization problem of a structural overall stiffness subject to the volume constraint. Moreover, for some structures such as an aircraft wing, the displacements of the exterior surface should remain within a certain limit in order to maintain the aerodynamic performance (Sobieski and Haftka 1997).

To obtain a predominantly black-and-white optimal topology along the approximate binary path of the structural topology optimization, an improved displacement constrained topology optimization method of continuum structures is proposed. The structure of this paper is organized as follows. In Section 2, a feature of constraint displacement derivatives is introduced and analyzed. In Section 3.1 and 3.2, an improved approximate model with constraint limit adjustments and a volume penalty objective function, is proposed for the displacement constraint problem under multiple load cases. In Section 3.3, an adaptive approach of adjusting design variable bounds is proposed and integrated into the approximate model with varied constraint limits. In Section 4, a smooth dual algorithm of the approximate problem is developed. And a filtering scheme, a stabilization operation, and a stopping

iteration criterion are given in Sections 5 and 6. The numerical results, analyses and a conclusion of the proposed method are given in Sections 7 and 8.

2 A feature of displacement derivatives

In this paper, the binary topological variable ρ_i(i.e., relative density) is replaced by the continuous topological variable ρ_i that varies between $\rho_i^{min} = 0.00001$ and 1. The volume and stiffness matrix expressions of a structural element are given as follows:

$$V_i = f_v(\rho_i)V_i^0, \quad \mathbf{K}^i = f_k(\rho_i)\mathbf{K}_0^i \qquad (1)$$

where V_i and $\mathbf{K}^i$ are the volume and stiffness matrices of the ith element, respectively. And V_i^0 and $\mathbf{K}_0^i$ are the original volume and stiffness matrices of the ith element, respectively. ρ_i is the topology variable of the ith element. And $f_v(\rho_i)$ and $f_k(\rho_i)$ denote the interpolation (identification or penalty) functions of the volume and stiffness matrices of the ith element, respectively.

Being referred to the RAMP model (Stolpe and Svanberg 2001a), interpolation functions $f_k(\rho_i) = \rho_i/(1 + \upsilon(1 - \rho_i))$ and $f_v(\rho_i) = \rho_i^{\alpha_v}$ are selected. Being referred to (18) of Wood and Groenwold (2010), $\alpha_v \leq 1.0$ denotes the penalty parameter, and a penalty is introduced into the volume objective function. Some references(Stolpe and Svanberg 2001a, Wood and Groenwold 2010 and etc.)showed that $\upsilon = 6.0$ and $\alpha_v = 0.8$ are appropriate for obtaining an optimal topology. And $\upsilon = 6.0$ and $\alpha_v = 0.8$ are also used in this paper examples.

Figure 1 gives a cantilever beam under a plane stress condition. The left hand side of the beam is fixed. A vertical load of $3kN$ is applied at the middle point of the free end. The dimension of the beam is $0.32\,m \times 0.16m \times 0.001m$. The Young's modulus $E = 200\,GPa$and Poisson's ratio $\nu = 0.33$ are specified. The maximum design domain is divided into a mesh of 64×32 with 2048 equal-size four-node square plane stress elements. Displacement constraints are imposed on the vertical displacement $u_{ay}(\boldsymbol{\rho})$ at the middle point of the free end and the vertical displacement $u_{qy}(\boldsymbol{\rho})$ at the point of interest 'q' located in the middle of the top edge of the beam in Fig. 1, respectively. Where $\boldsymbol{\rho}$ is a topological variable vector.
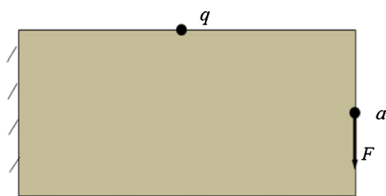

Fig.1 A single-load problem with displacement constraints for a cantilever beam

A displacement derivative with respect to the topological variable ρ_i can be expressed as

$$
\begin{aligned}
\partial\left|u_{ay}\left(\boldsymbol{\rho}^{(0)}\right)\right| / \partial\rho_i &= \lim_{\boldsymbol{\rho}\to\boldsymbol{\rho}^{(0)}} \left(\left|u_{ay}(\boldsymbol{\rho})\right| - \left|u_{ay}\left(\boldsymbol{\rho}^{(0)}\right)\right|\right) / \left(\rho_i - \rho_i^{(0)}\right) \\
&= \left[\lim_{\boldsymbol{\rho}\to\boldsymbol{\rho}^{(0)}} \left(u_{ay}^2(\boldsymbol{\rho}) - u_{ay}^2\left(\boldsymbol{\rho}^{(0)}\right)\right) / \left(\rho_i - \rho_i^{(0)}\right)\right] \\
&\quad \Big/ \lim_{\boldsymbol{\rho}\to\boldsymbol{\rho}^{(0)}} \left(\left|u_{ay}(\boldsymbol{\rho})\right| + \left|u_{ay}\left(\boldsymbol{\rho}^{(0)}\right)\right|\right) \\
&= \left(2u_{ay}\left(\boldsymbol{\rho}^{(0)}\right)\partial u_{ay}\left(\boldsymbol{\rho}^{(0)}\right) / \partial\rho_i\right) / \left(2\left|u_{ay}\left(\boldsymbol{\rho}^{(0)}\right)\right|\right) \\
&= sign\left(u_{ay}\left(\boldsymbol{\rho}^{(0)}\right)\right)\partial u_{ay}\left(\boldsymbol{\rho}^{(0)}\right) / \partial\rho_i
\end{aligned}
\tag{2}
$$

where $u_{ay}(\boldsymbol{\rho}^{(0)}) \neq 0.0$.

Therefore, $\partial|u_{ay}(\boldsymbol{\rho}^{(0)})|/\partial\rho_i$ easily is obtained by using the second expression of (1), seeing the paper provided by Huang and Xie (2010). In this paper, a sensitivity filtering approach similar to it proposed by Sigmund (2001), is adopted to deal with numerical instabilities (Sigmund and Peterson 1998) in topology optimization. Fig. 2a gives a topology variable distribution of the beam. And Fig. 2b and Fig. 2c depict the logarithmic distributions of the ratios between the absolute values of filtered constraint displacement derivatives and the absolute values of corresponding displacements at the constraint directions of the structure in Fig. 2a, respectively. Here, filtered constraint displacement derivatives mean that the constraint displacement derivatives are modified by use of the filtering approach.

It is found from Fig. 2b, c that there are huge differences between the maximums and corresponding minimums of the absolute values of these displacement derivatives within all the structural elements in the structures of Fig. 2b and Fig. 2c, respectively. For example, the ratios of these maximums and corresponding minimums, obtained by numerical computations, are 3.80×10^6 and 4.54×10^7 in the structures of Fig. 2b and Fig. 2c, respectively. And for some constraint structural displacement under a load case, there also exist some structural regions including elements that possess relative small absolute values of displacement derivatives with respect to their maximum. Here, the aforementioned huge difference and some structural regions with relative small absolute values of displacement derivatives in a structure, are thought as a feature of structural displacement derivatives.

The load case in Fig. 1 is replaced by another load case, in which a uniform distributed load of $600kN/m$ is applied on the free end of the beam along the vertical direction. The logarithmic $\ln(|\partial u_{ay}(\boldsymbol{\rho})|/\partial\rho_i|/|u_{ay}(\boldsymbol{\rho})|)$ distribution of the ratios between the absolute values of

(a)   (b)   (c)
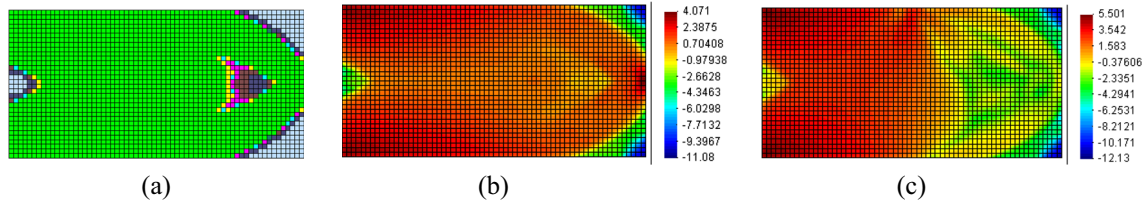
Fig. 2 A topology variable distribution, and the logarithmic distributions of the ratios between the absolute values of filtered constraint displacement derivatives and the absolute values of corresponding vertical displacements, respectively, at the middle point "a" of the free end and the "q" point of the top side of the beam in Fig.1, corresponding to Fig.2a: (**a**) topology variable distribution; (**b**) derivatives logarithmic $\ln(|\partial|u_{ay}(\boldsymbol{\rho})|/\partial\rho_i|/|u_{ay}(\boldsymbol{\rho})|)$ distributions with respect to topology variables; (**c**) derivatives logarithmic $\ln(|\partial|u_{qy}(\boldsymbol{\rho})|/\partial\rho_i|/|u_{qy}(\boldsymbol{\rho})|)$ distributions with respect to topology variables. Note: In Fig.2a and color topology variable distributions of the consequent sections, the greenest elements denote elements whose topology variable values all are between 0.95 and

1.0; the dark green elements denote elements whose topology variable values all are between 0.9 and 0.95;the yellow elements denote elements whose topology variable values all are between 0.7 and 0.9; the blueish elements denote elements whose topology variable values all are between 0.5 and 0.7; the red elements denote elements whose topology variable values all are between 0.3 and 0.5; the dark red elements denote elements whose topology variable values all are between 0.1 and 0.3; the darkish elements denote elements whose topology variable values all are between 0.001 and 0.1; the silver white elements denote elements whose topology variable values all are below 0.001. $|\bullet|$ denotes the absolute value of $\bullet$

filtered constraint displacement derivatives and the absolute value $|u_{ay}(\boldsymbol{\rho})|$ of the vertical displacement at the middle point of the free end of the beam under the uniform distributed load case, is shown in Fig.3. The physical feature in Fig. 2 also occurs in Fig. 3. Generally, the constraint displacement function $|u_{ay}(\boldsymbol{\rho})|$ in Fig. 2 or Fig. 3 can approximately be expressed as an one-order Taylor series expansion, namely

$$\left|u_{ay}(\boldsymbol{\rho})\right| \approx \left|u_{ay}\left(\boldsymbol{\rho}^{(k-1)}\right)\right|$$
$$+ \sum_{q=1}^{Q} \frac{\partial\left|u_{ay}\left(\boldsymbol{\rho}^{(k-1)}\right)\right|}{\partial\rho_{n_q}}\left(\rho_{n_q}-\rho_{n_q}^{(k-1)}\right) \quad (3)$$

where,Q is the number of the designable elements, and the designable element numbering may be represented by n_q , $q = 1,2,\cdots,Q$. It is assumed that a few (such as $\overline{n} = 0.015Q$, i.e. a small value with respect to Q) elements with the minimum absolute values of one-order displacement derivatives within the elements whose topology variables are bigger than 0.1 in Fig. 2 or Fig. 3, are selected. And their topology variables are denoted by $\rho_{n_{ql}}, l = 1,2,\cdots,\overline{n}$. Where,

Fig. 3 The logarithmic $\ln(|\partial|u_{ay}(\boldsymbol{\rho})|/\partial\rho_i|/|u_{ay}(\boldsymbol{\rho})|)$ distribution of the ratios between the absolute values of filtered constraint displacement derivatives and the absolute value $|u_{ay}(\boldsymbol{\rho})|$ of the vertical displacement at the middle point "a" of the free end of the beam, where topology variables all are equal to 1.0

$\left\{n_{ql}, l = 1,2,\cdots,\overline{n}\right\}$ is a subset of $\{nq, q = 1,2,\cdots,Q\}$. It is assumed that there exist big changes (such as $\rho_{n_{ql}}$ from $\rho_{n_{ql}}^{(k-1)}$ to $\rho_{n_{ql}}^{\min} = 0.00001$) of the topology variables $\rho_{n_{ql}}, l = 1,2,\cdots\overline{n}$, and topology variables of other elements in the structure are kept as constants. From (3), one total change quantity of the displacement function can approximately be estimated as follows.

$$\left|\Delta\left|u_{ay}(\boldsymbol{\rho})\right|\right| \approx \left|\sum_{l=1}^{\overline{n}}\left(\rho_{n_{ql}}^{\min}-\rho_{n_{ql}}^{(k-1)}\right)\frac{\partial\left|u_{ay}\left(\boldsymbol{\rho}^{(k-1)}\right)\right|}{\partial p_{n_{ql}}}\right| \leq 2.0$$
$$\times \sum_{l=1}^{\overline{n}}\left|\frac{\partial\left|u_{ay}\left(\boldsymbol{\rho}^{(k-1)}\right)\right|}{\partial p_{n_{ql}}}\right| \quad (4)$$

From Fig. 2 and Fig. 3, it can easily be known that the term at the right-hand side of (4) is a very small quantity with respect to $|u_{ay}(\boldsymbol{\rho})|$. Therefore, big changes of topology variables of these elements have a little effect on the structural constraint displacement $|u_{ay}(\boldsymbol{\rho})|$. In view of volume minimizing, if a small quantity addition (such as $0.01|u_{ay}(\boldsymbol{\rho})|$) on the constraint point displacement value $|u_{ay}(\boldsymbol{\rho})|$ of the current design, is allowed, these $\overline{n}$ elements will be removed, and topology variables of other elements will not be changed. Namely, if a small quantity addition on the constraint point displacement value $|u_{ay}(\boldsymbol{\rho})|$ of the current design is imposed on the optimization model, it may explanatively be justified that this element change way approximately follows the binary path of the structural topology optimization at the current iteration. It also may empirically be justified from Fig. 2 and Fig. 3 that the aforementioned feature of displacement derivatives just is the essential foundation of the success of the ESO and BESO methods.
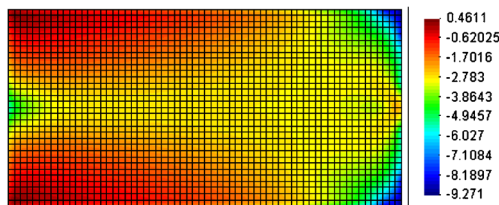
3 A structural optimization model and its novel approximate model

3.1 Problem statement

In this study, a fixed maximum finite element mesh is adopted. Structural elements can be categorized into two kinds: (a) designable elements and (b) non-designable elements. The non-designable element numbering may be expressed as $i_p, p = 1, 2, \cdots, P$, its topological variables $\rho_{i_p}, p = 1, 2, \cdots, P$ do not change during the optimization process, and P is the number of the non-designable elements. The designable element numbering may be represented by $n_q, q = 1, 2, \cdots, Q$, and Q is the number of the designable elements. The displacement constrained optimization problem is formulated as follows.

$$\begin{cases} \min \quad V = \sum_{q=1}^{Q} \rho_{n_q}^{\alpha_v} V_{n_q}^0 + \sum_{p=1}^{P} \rho_{i_p}^{\alpha_v} V_{i_p}^0 \\ s.t. \quad \left| u_{NC_j}^l(\boldsymbol{\rho}) \right| \leq U_j, \quad j = 1, 2, \cdots, J; \ l = 1, 2, \cdots, L \quad (5) \\ \qquad \mathbf{K}(\boldsymbol{\rho}) \, \mathbf{u}^l(\boldsymbol{\rho}) = \mathbf{F}^l \\ \qquad \rho_{n_q}^{\min} \leq \rho_{n_q} \leq 1, \quad q = 1, 2, \cdots, Q \end{cases}$$

where V is the structural volume, and $V_{n_q}^0$ and $V_{i_p}^0$ are the original volumes of the n_q-th element and the i_p-th element, respectively. $\mathbf{K}(\boldsymbol{\rho})$ is the structural total stiffness matrix, $\mathbf{F}^l$ is the lth load acting on the structure, and $\mathbf{u}^l(\boldsymbol{\rho})$ is the displacement vector under the lth load case. And L is the number of the load cases. $u_{NC_j}^l(\boldsymbol{\rho})$ is the displacement at the NC_j-th degree of freedom of the structure under the lth load case. And U_j is the constraint limit of the jth displacement constraint. J is the number of the displacement constraints for each load case. ρ_{n_q} is the qth topological variable, and $\rho_{n_q}^{\min}$ is its lower limit, and $\rho_{n_q}^{\min} = 0.00001$ is used in the examples of this paper. In order to deal with the checkerboard problem of topology optimization, a displacement sensitivity filtering approach is adopted to modify displacement sensitivities.

3.2 An improved approximate model with varied constraint limits

In engineering structural optimization, an objective function or/and constraint functions (including structural mechanics behaviors) are nonlinear functions of design variables, and also are implicit functions of design variables. Generally speaking, at each iteration of an optimization process, an approximate optimization model replaces its original structural optimization model, in which approximate explicit functions replace their original implicit objective and constraint functions (Nocedal and Wright 1999, Sigmund and Maute 2013, and Deaton and Grandhi 2014). An approximate optimization model should approximately be equivalent to the original structural optimization model in a certain domain of the current design point. The original structural optimization model possesses at least two performances: (a) the change requirements of its objective function and constraint functions can strongly control the change domain of design variables; (b) design variable changes within a small domain, can make that the objective function and constraint functions change in a small quantity way. Moreover, if a series of topologies with clear profiles must be obtained during an optimization process, the proposed optimization method should possess a feature. This feature is that the topology variables of only a few of elements are allowed to change within a large range at each iteration step. Namely, this feature requirement must be imposed on its approximate model or its algorithm at most iteration steps. A lot of simulations demonstrate that varied displacement limits are beneficial to big changes of topology variables of only a few of elements at each iteration step. At same time, these limits also can make that Lagrange multipliers of the approximate model possess at least one non-zero value in the case of approximate binary changes of only a few of design variables to a certain extent, even if at many beginning iteration steps when the maximum design domain filled with solid material is selected as its initial design.

An approximate optimization model with varied displacement constraint limits, is constructed as follows:

$$\begin{cases} \min \quad \sum_{q=1}^{Q} \rho_{n_q}^{\alpha_v} V_{n_q}^0 \Big/ V^{(0)} \\ s.t. \quad \left| \tilde{u}_{NC_j}^l(\boldsymbol{\rho}) \right| \Big/ \left| u_{NC_j}^{l,(0)} \right| \leq \tilde{U}_j^{(k)} \Big/ \left| u_{NC_j}^{l,(0)} \right|, \quad j = 1, 2, \cdots, J; l = 1, 2, \cdots, L; k = 1, 2, \cdots \\ \qquad \rho_{n_q}^{\min} \leq \rho_{n_q} \leq 1, \quad q = 1, 2, \cdots, Q \end{cases} \quad (6)$$

where $\left| \tilde{u}_{NC_j}^l(\boldsymbol{\rho}) \right|$ denotes a one-order Taylor series expansion of $\left| u_{NC_j}^l(\boldsymbol{\rho}) \right|$ at $\rho_{n_q}^{(k-1)}, q = 1, 2, \cdots, Q$, and $\left| u_{NC_j}^{l,(0)} \right|$ is its initial value, and $V^{(0)}$ is the initial design structural volume. The varied displacement limit $\tilde{U}_j^{(k)}$ at the kth iteration is

introduced and expressed as

$$\tilde{U}_j^{(k)} = \overline{U}_j^{(k)}, \quad j = 1, \cdots, J; \quad k = 1 \tag{7}$$

$$\tilde{U}_j^{(k)} = \begin{cases} \max\left(\overline{U}_j^{(k)}, U_j^{(k)}\right), & \text{if } \max\limits_{l=1,2,\cdots,L}\left(\left|u_{NC_j}^{l,(0)}\right|\right) \leq U_j \\ \min\left(\overline{U}_j^{(k)}, U_j^{(k)}\right), & \text{if } \max\limits_{l=1,2,\cdots,L}\left(\left|u_{NC_j}^{l,(0)}\right|\right) > U_j \end{cases}, \quad j = 1,\cdots,J; k = 2,3,\cdots \tag{8}$$

where, $\overline{U}_j^{(k)}$ and $U_j^{(k)}$ are given by use of following formulas.

$$\overline{U}_j^{(k)} = \begin{cases} \min\left(\left(\max\limits_{l=1,2,\cdots,L}\left(\left|u_{NC_j}^{l,(k-1)}\right|\right) + \beta_1\eta_j U_j\right), U_j\right), & \text{if } \max\limits_{l=1,2,\cdots,L}\left(\left|u_{NC_j}^{l,(0)}\right|\right) \leq U_j \\ \max\left(\left(\max\limits_{l=1,2,\cdots,L}\left(\left|u_{NC_j}^{l,(k-1)}\right|\right) - \beta_1\eta_j U_j\right), U_j\right), & \text{if } \max\limits_{l=1,2,\cdots,L}\left(\left|u_{NC_j}^{l,(0)}\right|\right) > U_j \end{cases}; j = 1,\cdots,J; k = 1,2,\cdots \tag{9}$$

$$U_j^{(k)} = \begin{cases} \min\left(\left(\tilde{U}_j^{(k-1)} + \beta_1\eta_j U_j\right), U_j\right), & \text{if } \max\limits_{l=1,2,\cdots,L}\left(\left|u_{NC_j}^{l,(0)}\right|\right) \leq U_j \\ \max\left(\left(\tilde{U}_j^{(k-1)} - \beta_1\eta_j U_j\right), U_j\right), & \text{if } \max\limits_{l=1,2,\cdots,L}\left(\left|u_{NC_j}^{l,(0)}\right|\right) > U_j \end{cases}, \quad j = 1,\cdots,J; k = 2,3,\cdots \tag{10}$$

$$\eta_j = \min\left\{ \frac{\min\limits_{l=1,\cdots,L}\left(\left|U_j - \left|u_{NC_j}^{l,(0)}\right|\right|\right)}{\min\limits_{l=1,\cdots,L; j=1,2,\cdots,J}\left(\left|U_j - \left|u_{NC_j}^{l,(0)}\right|\right|\right)}, 1.5 \right\}, j = 1,\cdots,J \tag{11}$$

where $u_{NC_j}^{l,(k-1)}$ is the displacement at the NC_j-th degree of freedom of the structural topology obtained at the $(k\text{-}1)$th outer loop iteration step under the lth load case. η_j is a displacement limit ratio factor, and $\eta_j \geq 1.0$ for $j = 1, 2, \cdots, J$. β_1 is a displacement limit empirical parameter, and one value of $[0.002, 0.012]$ is selected as β_1 in the examples of this paper. Here, the varied displacement limit scheme given by (7-11) is different from the varied limit scheme proposed by Rong and Yi (2010), Rong et al. (2011). For example, for approximate optimization model (6) with $\max\limits_{l=1,2,\cdots,L}\left(\left|u_{NC_j}^{l,(0)}\right|\right) \leq U_j, j = 1, 2, \cdots, J$, there always exists a limited integer number k_0 ($k_0 \in \{1, 2, \cdots, k, \cdots\}$, and k_0 is a constant for the prescribed β_1 and displacement limits $U_j, j = 1, 2, \cdots, J$) so that the following (12, 13) can be guaranteed by adopting the varied displacement limit $\tilde{U}_j^{(k)}$ in (7, 8) and (9, 10).

$$U_j = \cdots = \tilde{U}_j^{(k_0+1)} = \tilde{U}_j^{(k_0)} \geq \cdots > \tilde{U}_j^{(k+1)} > \tilde{U}_j^{(k)}$$
$$> \tilde{U}_j^{(k-1)} > \cdots > \tilde{U}_j^{(2)} > \tilde{U}_j^{(1)}, \quad j = 1,\cdots,J \tag{12}$$

$$\Omega_{fd} = \cdots = \Omega_{(k_0+1)}$$
$$= \Omega_{(k_0)} \supset \cdots \supset \Omega_{(k+1)} \supset \Omega_{(k)} \supset \Omega_{(k-1)} \supset \cdots \supset \Omega_{(2)} \supset \Omega_{(1)} \tag{13}$$

where $\Omega_{(k)}$ ($k \geq 1$) denotes the feasible domain of the approximate optimization model (6) at the kth iterative step in Fig. 4.

Now, the feature of the model (6) is introduced. Fig. 4 gives a simple interpretation of optimization iteration solutions for the model (6) when $\max\limits_{l=1,2,\cdots,L}\left(\left|u_{NC_j}^{l,(0)}\right|\right) \leq U_j, j = 1, 2, \cdots, J$. $\rho^{(k-1)}$, $\rho^{(k)}$ and $\rho^{(k+1)}$, $k \geq 2$ in Fig. 4, respectively, represent the solutions obtained by adopting the proposed method at the $(k\text{-}1)$th, kth and $(k+1)$th iteration steps. And Ω_{fd} and
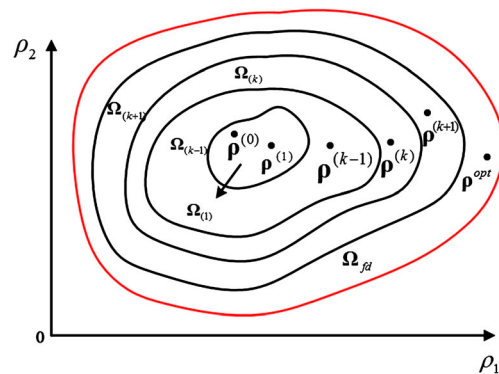

Fig. 4 A simple illustration of optimization iteration solutions for the model (6)

ρ^{opt} represent the feasible domain and an optimal solution of the original optimization model (5) in Fig. 4, respectively.

The feasible domain Ω_{fd} of the original optimization model (5) may be divided into a feasible domain $\Omega_{(k)}$ and a non-feasible sub-domain $(\Omega_{fd} - \Omega_{(k)})$ of the approximate model (6) at the kth iteration step because (12, 13) is satisfied. Namely, a feasible sub-domain $(\Omega_{fd} - \Omega_{(k)})$ of the original model (5) may become a non-feasible sub-domain of the approximate model (6) at the kth iteration step. And a non-feasible sub-domain $(\Omega_{(k+1)} - \Omega_{(k)})$ of the approximate model (6) at the kth iteration step may become a feasible sub-domain of the approximate model (6) at the $(k+1)$-th iteration step.

Therefore, the varied displacement limit parameter β_1 of the (7-11) may be manipulated to make that the model (6) possesses a smaller feasible domain $\Omega_{(k)}$ shown in Fig. 4 than the model (5). The optimal solution within $\Omega_{(k)}$ and the next iteration solution $\rho^{(k)}$ of the model (6) will fall in a smaller local feasible domain $(\Omega_{(k)} - \Omega_{(k-1)})$ shown in Fig. 4 at the kth iteration step because of the volume minimizing requirement, the varied displacement limits in (7-11), and the features of Section 2. It is found from simulations that the approximate model (6) with more tight displacement constraints at all iteration steps, the smaller local feasible domain $\Omega_{(k)}$, and the features of Section 2, can provide very strong effect to enhance the robustness of an optimization process and black/white distributions of a series of topologies obtained.

Moreover, for $\max\limits_{l=1,2,\cdots,L} \left(\left| u_{NC_j}^{l,(0)} \right| \right) \leq U_j$ or $\max\limits_{l=1,2,\cdots,L} \left(\left| u_{NC_j}^{l,(0)} \right| \right) > U_j$, it can easily be found from (6–13) that the feasible domain of an approximate optimization model after a limited iteration step (such as k_0) of an optimization process, is completely coincided with the feasible domain of the original model. If a mathematical programming algorithm is adopted to solve the models (6), the convergence of the algorithm for the approximate model (6) may completely be determined by the algorithm performance. The scheme of the (7, 8) and (9, 10), is a modification of the varied limit scheme proposed by Rong and Yi (2010), Rong et al. (2011).

3.3 An adaptive approach of adjusting design variable bounds

3.3.1 The case of at least one non-zero Lagrange multiplier

Gradient-based optimization algorithms that rely on nonlinear but convex separable quadratic approximation functions, have been proven to be very effective for large-scale structural optimization (see, e.g. Groenwold and Etman 2009; Groenwold et al. 2009). Fleury (1989) proposed a SQP(Sequential quadratic programming)method that uses diagonal Hessian information only. The conservative convex separable approximation (CCSA) framework proposed by Svanberg (1987) may be used to ensure a global convergence and termination. Wood and Groenwold (2010) investigated the topology optimization problem with SIMP-like volumetric penalization, in which minimum compliance is sought subject to a single concave constraint on the volume. They showed that it is sometimes possible to solve non-convex problems directly using a dual method. They also concluded that the presence of the concave constraint may increase the difficulty of the problem dramatically if one employs a method based on strictly convex approximations. Their numerical results exhibited large-scale oscillatory behaviors of physical quantities during an optimization process unless an additional external move limit was applied.

Moreover, $\partial^2 \left| u_{NC_j}^l(\rho) \right| / \partial \left(\rho_{n_q} \right)^2$ at some design points with partial small topology variable values, may be negative. Namely, the quadratic Taylor series expansion of $\left| u_{NC_j}^l(\rho) \right|$ with respect to topology variables may be a non-convex function in a small region of some design point with partial small topology variable values. If separable strict convex quadratic approximations of the constraints $\left| u_{NC_j}^l(\rho) \right| / \left| u_{NC_j}^{l,(0)} \right| \leq \tilde{U}_j^{(k)} / \left| u_{NC_j}^{l,(0)} \right|$ replace displacement constraints of the model (6), (13) can not be guaranteed by these approximation

(a) Outer loop iteration 5

(b) Outer loop iteration 15

(c) Outer loop iteration 25

(d) Outerloop iteration 40

(i) Outer loop iteration 70

(j) Outer loop iteration 80

(k) Outer loop iteration 88

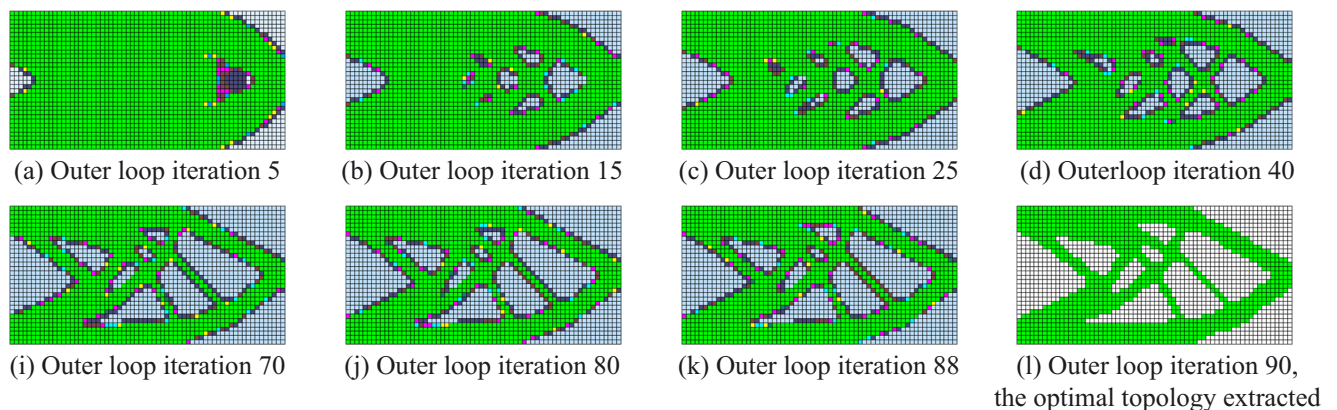(l) Outer loop iteration 90, the optimal topology extracted

Fig. 5 The topology distribution optimization history of the cantilever beam, which is obtained by the proposed method for the volume penalty parameter $\alpha_v=1.0$, and $d_a=1.5$ and $d_q=1.5$. Note: In Fig. 5 (l), the white elements denote elements whose topology variable values are equal to 0.00001
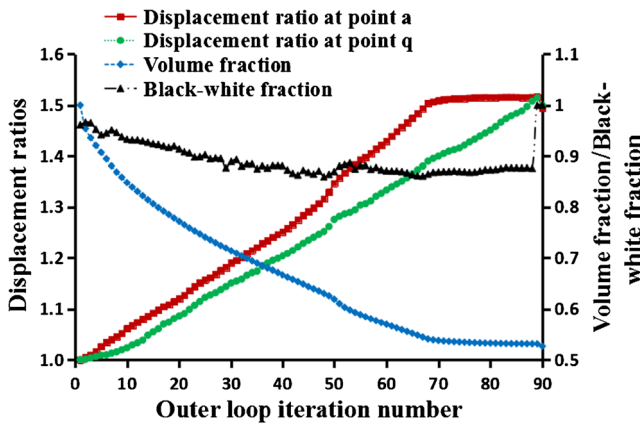
Fig. 6 The volume fraction, black and white fraction and displacement ratio optimization histories of the cantilever beam, which is obtained by the proposed method for the volume penalty parameter α_v=1.0, and d_a=1.5 and d_q=1.5

constraints, when a lot of elements of the optimized structure possess small topology variable values.

Here, topology variables are selected as design variables, and the varied constraint limit scheme of the (7-11), and one-order Taylor series expansions of displacement constraints are adopted in the approximate model (6). Namely, the approximate model (6) replaces the model (5) at each iteration step. However, the approximate displacement constraint functions and the objective function of the model (6) do not possess strong controlling ability of the topology variable changes. Some simulations also demonstrate that the approximate model (6) still do not completely possess the two performances aforementioned (at least one non-zero Lagrange multiplier in (14)), and also can not satisfy the requirement aforementioned in Section 3.2 at the most iteration steps.

$$
\begin{aligned}
L(\boldsymbol{\rho}, \boldsymbol{\lambda}) = &\sum_{q=1}^{Q} \rho_{n_q}^{\alpha_v} V_{n_q}^0 \Big/ V^{(0)} \\
&+ \sum_{l=1}^{L} \sum_{j=1}^{J} \lambda_{(l-1)\times J+j} \left(\left| \tilde{u}_{NC_j}^{l}(\boldsymbol{\rho}) \right| - \tilde{U}_j^{(k)} \right) \Big/ \left| u_{NC_j}^{l,(0)} \right|
\end{aligned}
$$
$$(14)$$

Therefore, in order to simply obtain a series of topologies with clear profiles during an optimization process, except that the approximate model (6) is adopted, change restrictions of the design variables are given so that the approximate model (6) possesses the two performances and the requirement

aforementioned in Section 3.2 at the most iteration steps. Generally speaking, the change region $\left[x_i^L, x_i^U\right]$ of any design variable x_i in trust region optimization methods, may be determined by using the objective and constraint function values and their derivative values at continuous several iteration steps (Tang 2014). Here, in order to effectively and simply construct trust regions of a lot of design variables, a novel trust region scheme being different from that of the paper published by Rong et al. (2016),is proposed.

(a) The basic characteristics of an optimal solution

It is assumed that $\{n_1, n_2, \cdots, n_q, \cdots, n_Q\}$ is denoted by a set $\boldsymbol{Q}$. When a structural optimization solution has evolved its optimal state, (15) should approximately be satisfied according to the KKT condition, and the approximate model (6) should possess at least one non-zero Lagrange multiplier (because of a non-zero volume derivative for any element with a topology variable value being close to 1.0). Therefore, increasing the topology variables of some design elements with the most minimum values of $\left|\partial L(\boldsymbol{\rho}, \boldsymbol{\lambda})/\partial \rho_{n_q}\right|$ in (15) within $\boldsymbol{Q}$, and reducing the topology variables of some design elements with the most minimum values of $\left|\partial L_{ca}(\boldsymbol{\rho}, \boldsymbol{\lambda})/\partial \rho_{n_q}\right|$ in (16) within $\boldsymbol{Q}$, will be beneficial to obtaining the optimal topology .

$$
\partial L(\boldsymbol{\rho}, \boldsymbol{\lambda}) \Big/ \partial \rho_{n_q} \approx 0.0, \quad n_q \in \boldsymbol{Q}
$$
$$(15)$$

$$
\partial L_{ca}(\boldsymbol{\rho}, \boldsymbol{\lambda}) \Big/ \partial \rho_{n_q} \approx \sum_{l=1}^{L} \sum_{j=1}^{J} \lambda_{(l-1)\times J+j} \left(\partial \left| u_{NC_j}^{l}\left(\boldsymbol{\rho}^{(k-1)}\right) \right| \Big/ \partial \rho_{n_q} \right) \Big/ \left| u_{NC_j}^{l,(0)} \right|
$$
$$(16)$$

where, $L(\boldsymbol{\rho}, \boldsymbol{\lambda})$ is the Lagrange function of the model (6), and $L_{ca}(\boldsymbol{\rho}, \boldsymbol{\lambda})$ is called as the Lagrange penalty function of the model (6).

(b) A novel trust region scheme

When there exists at least one non-zero Lagrange multiplier at the previous iteration step, i.e. the $(k\text{-}1)$ iteration step, $\lambda_{(l-1)\times J+j}, j=1,2,\cdots,J; l=1,2,\cdots,L$ in the (15, 16) are replaced by the Lagrange multipliers $\lambda(l-1) \times J + j(k-1)$ ($j=1, 2, \cdots, J; l=1, 2, \cdots, L$) obtained at the $(k\text{-}1)$th iteration step.

At first, a small empirical parameter δ_1 is prescribed, and a value of $[0.003, 0.012]$ is adopted as δ_1. At each iteration step,

Table 1 The characteristic data corresponding to the topologies in Fig.5

Numbering	(a)	(b)	(c)	(d)	(e)	(f)	(g)	(h)
$\left|u_{a_y}(\boldsymbol{\rho}^{(k)})\right| / \left|u_{a_y}(\boldsymbol{\rho}^{(0)})\right|$	1.034	1.098	1.161	1.258	1.511	1.515	1.516	1.494
$\left|u_{q_y}(\boldsymbol{\rho}^{(k)})\right| / \left|u_{q_y}(\boldsymbol{\rho}^{(0)})\right|$	1.010	1.061	1.127	1.208	1.405	1.458	1.510	1.501
Volume fraction	0.894	0.799	0.735	0.662	0.537	0.532	0.531	0.526
Black-white fraction	0.945	0.922	0.895	0.872	0.870	0.874	0.876	1.000

(a) Outer loop iteration 5   (b) Outer loop iteration 15   (c) Outer loop iteration 25   (d) Outer loop iteration 40

(i) Outer loop iteration 60   (j) Outer loop iteration 70   (k) Outer loop iteration 82   (l) Outer loop iteration 84, the optimal topology extracted
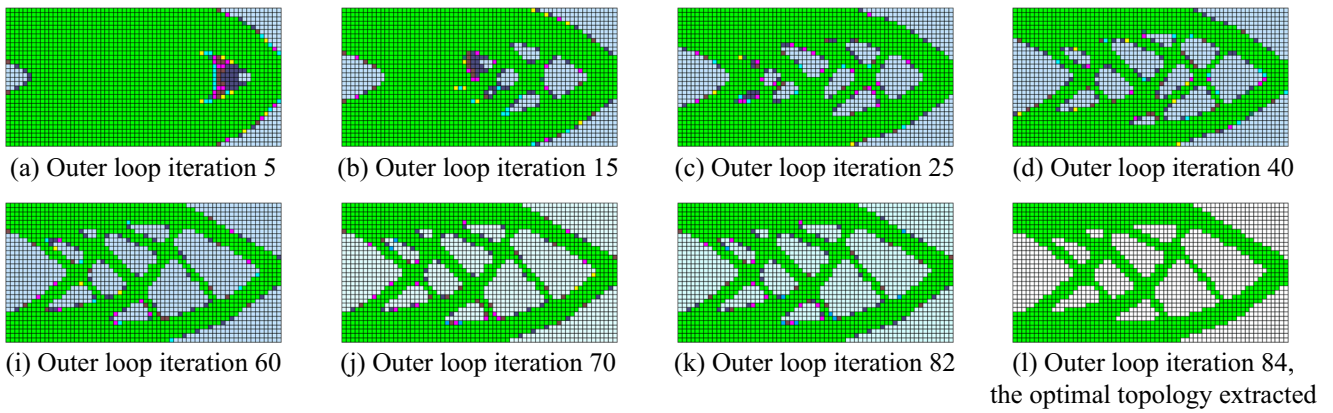
Fig. 7 The topology distribution optimization history of the cantilever beam, which is obtained by the proposed method for the volume penalty parameter α_v=0.8, and d_a=1.5 and d_q=1.5

the set Q with Q design elements, is divided into following four sub-sets:

(1) Constructing a design element subset $\mathbf{Q}_1$ with int($\delta_1 \times Q$) elements

Topology variables of elements in the subset $\mathbf{Q}_1$ all are bigger than 0.01, and will be reduced, and these int($\delta_1 \times Q$) elements possess the most minimum values of $\left|\partial L_{ca}(\boldsymbol{\rho}, \boldsymbol{\lambda})/\partial \rho_{n_q}\right|$ in (16) within $\boldsymbol{Q}$.

(2) Forming a design element subset $\mathbf{Q}_2$ with int($\delta_1 \times Q$) elements

Topology variables of elements in the subset $\mathbf{Q}_2$ all are between 0.01 and 0.999, and will be increased, and these int($\delta_1 \times Q$) elements possess the most minimum values of $\left|\partial L(\boldsymbol{\rho}, \boldsymbol{\lambda})/\partial \rho_{n_q}\right|$ in (15) within $(\mathbf{Q} - \mathbf{Q}_1)$.

(3) Constructing another design element subset $\mathbf{Q}_3$

All elements in the subset $\mathbf{Q}_3$ belong to the subset $(\mathbf{Q} - \mathbf{Q}_1 - \mathbf{Q}_2)$, their topology variables all are below 0.999, and will be changed.

(4) Forming the fourth element subset $\mathbf{Q}_4$

$\mathbf{Q}_4 = \mathbf{Q} - \overset{3}{\underset{i=1}{\cup}} \mathbf{Q}_i$ is set, and topology variables of elements in the subset $\mathbf{Q}_4$ all are held as constants at the current iteration step.

At least one of $\mathbf{Q}_1$, $\mathbf{Q}_2$ and $\mathbf{Q}_3$ is a non-empty set, and anyone of these three subsets may be an empty set at each iteration step. And following relations are satisfied.

$$\mathbf{Q} = \overset{4}{\underset{i=1}{\cup}} \mathbf{Q}_i; \qquad \mathbf{Q}_i \cap \mathbf{Q}_j = \mathbf{0}, \quad i,j = 1,2,3,4; i \neq j \qquad (17)$$

where $\cap$ and $\cup$ represent the intersect set and sum set operators of several sets, respectively.

It is assumed that $\overline{n}_q, q = 1,2,\cdots,Q_{red}$ is the element numbering of the subset $\mathbf{Q}_1$, and Q_{red} is equal to int($\delta_1 \times Q$); $\tilde{n}_q, q = 1,2,\cdots,Q_{inc}$ is the element numbering of the subset $\mathbf{Q}_2$, and Q_{inc} is less than and equal to int($\delta_1 \times Q$); $\widetilde{\overline{n}}_q, q = 1,2,\cdots,Q_{cha}$ is the element numbering of the subset $\mathbf{Q}_3$, and Q_{cha} is its element number. In this paper, the topology variables $\rho_{\overline{n}_q}$ for any $\overline{n}_q \in \mathbf{Q}_1$, $\rho_{\tilde{n}_q}$ for any $\tilde{n}_q \in \mathbf{Q}_2$ and $\rho_{\widetilde{\overline{n}}_q}$ for any $\widetilde{\overline{n}}_q \in \mathbf{Q}_3$ are temporarily selected as design variables, and the topology variable ρ_{n_q} for any $n_q \in \mathbf{Q}_4$ is set as a constant at each iteration step.

Following formulas are directly adopted by use of the aforementioned scheme.

$$1.0 \times 10^{-5} = \rho_{\overline{n}_q}^L \leq \rho_{\overline{n}_q} \leq \rho_{\overline{n}_q}^U = 1.0, \quad \overline{n}_q \in \mathbf{Q}_1 \qquad (18)$$

$$1.0 \times 10^{-5} = \rho_{\tilde{n}_q}^L \leq \rho_{\tilde{n}_q} \leq \rho_{\tilde{n}_q}^U = 1.0, \quad \tilde{n}_q \in \mathbf{Q}_2 \qquad (19)$$
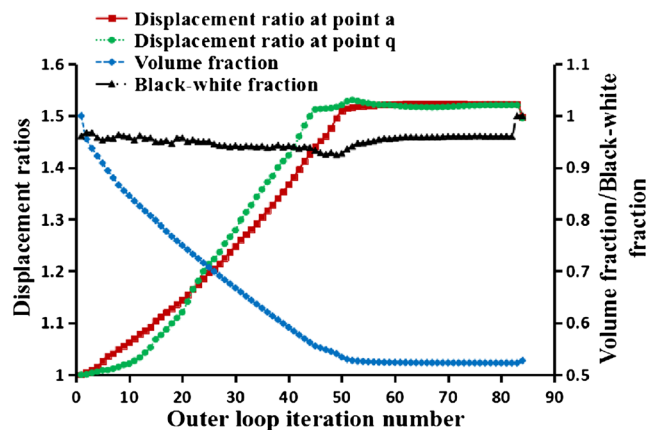

Fig. 8 The volume fraction, black and white fraction and displacement ratio optimization histories of the cantilever beam, obtained by the proposed method for the volume penalty parameter α_v=0.8, and d_a=1.5 and d_q=1.5

$$\max\left\{\left(\rho_{\widetilde{\overline{n}}_q}^{(k-1)}-\Delta\right),1.0\times10^{-5}\right\}=\rho_{\widetilde{\overline{n}}_q}^L\leq\rho_{\widetilde{\overline{n}}_q}\leq\rho_{\widetilde{\overline{n}}_q}^U$$

$$=\min\left\{\left(\rho_{\widetilde{\overline{n}}_q}^{(k-1)}+\Delta\right),\ 1.0\right\}\ ,\quad\widetilde{\overline{n}}_q\in\mathbf{Q}_3 \tag{20}$$

where, Δ may be treated as an empirical parameter, and a value of $[0.01,0.02]$ can be selected as Δ according to small variable region requirements in general trust region optimization methods (Nocedal and Wright 1999). $\Delta=0.015$ is adopted, and is not a sensitive parameter in all examples of this paper. Based on (18-20) and the aforementioned change scheme of design variables, the approximate model (6) may be transferred into the approximate model (21):

$$\begin{cases}\min & \left(\sum_{q=1}^{Q_{red}}\rho_{\overline{n}_q}^{\alpha_v}V_{\overline{n}_q}^0+\sum_{q=1}^{Q_{inc}}\rho_{\tilde{n}_q}^{\alpha_v}V_{\tilde{n}_q}^0+\sum_{q=1}^{Q_{cha}}\rho_{\widetilde{\overline{n}}_q}^{\alpha_v}V_{\widetilde{\overline{n}}_q}^0\right)\Big/V^{(0)}\\ s.t. & \left(\left|\tilde{u}_{NC_j}^l(\boldsymbol{\rho})\right|\Big/\left|u_{NC_j}^{l,(0)}\right|-\tilde{U}_j^{(k)}\Big/\left|u_{NC_j}^{l,(0)}\right|\right)\leq0.0\\ & \rho_{\overline{n}_q}\in\left[\rho_{\overline{n}_q}^L,\rho_{\overline{n}_q}^U\right],\quad\overline{n}_q\in\mathbf{Q}_1\\ & \rho_{\tilde{n}_q}\in\left[\rho_{\tilde{n}_q}^L,\rho_{\tilde{n}_q}^U\right],\quad\tilde{n}_q\in\mathbf{Q}_2\\ & \rho_{\widetilde{\overline{n}}_q}\in\left[\rho_{\widetilde{\overline{n}}_q}^L,\rho_{\widetilde{\overline{n}}_q}^U\right],\quad\widetilde{\overline{n}}_q\in\mathbf{Q}_3\end{cases},\quad\begin{array}{l}j=1,\cdots,J;l=1,2,\cdots,L;\\ k=1,2,\cdots\end{array} \tag{21}$$

3.3.2 The case of zero Lagrange multipliers

Some simulations show that the case of zero Lagrange multipliers of the model (21), will occur at a few of outer iteration steps during the early process of an optimization iteration solving, when a big value of β_1 in (9-11) is adopted. For the case of that Lagrange multipliers all are zero at the end of the (k-1)th iteration step (for example, the first iteration step), firstly setting

$$g_1^*\left(\boldsymbol{\rho}^{(k-1)}\right)=\left(\left|\tilde{u}_{NC_{j_s}}^{l_s}\left(\boldsymbol{\rho}^{(k-1)}\right)\right|\Big/\left|u_{NC_{j_s}}^{l_s,(0)}\right|-\tilde{U}_{j_s}^{(k)}\Big/\left|u_{NC_{j_s}}^{l_s,(0)}\right|\right) \tag{22}$$

where, l_s and NC_{j_s} satisfy following equation.

$$\left|\left(\left|\tilde{u}_{NC_{j_s}}^{l_s}\left(\boldsymbol{\rho}^{(k-1)}\right)\right|\Big/\left|u_{NC_{j_s}}^{l_s,(0)}\right|-\tilde{U}_{j_s}^{(k)}\Big/\left|u_{NC_{j_s}}^{l_s,(0)}\right|\right)\right|$$

$$=\min_{\substack{l=1,2,\cdots,L\\j=1,2,\cdots,J}}\left|\left(\left|\tilde{u}_{NC_j}^l\left(\boldsymbol{\rho}^{(k-1)}\right)\right|\Big/\left|u_{NC_j}^{l,(0)}\right|-\tilde{U}_j^{(k)}\Big/\left|u_{NC_j}^{l,(0)}\right|\right)\right| \tag{23}$$

For another prescribed small parameter δ_2, if (24) is satisfied, the displacement constraint function at the NC_j-th degree of freedom of the structure under the lth load case will be considered as a potential tight constraint.

$$\left|\left|\left(\left|\tilde{u}_{NC_j}^l\left(\boldsymbol{\rho}^{(k-1)}\right)\right|\Big/\left|u_{NC_j}^{l,(0)}\right|-\tilde{U}_j^{(k)}\Big/\left|u_{NC_j}^{l,(0)}\right|\right)\right|-\left|g_1^*\left(\boldsymbol{\rho}^{(k-1)}\right)\right|\right|\leq\delta_2 \tag{24}$$
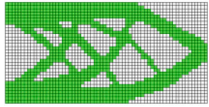
where, any value of an empirical parameter δ_2 within $[0.03,0.06]$ does not affect the final optimization solution and solving speed of the proposed method, because the proposed method makes that the objective function and constraint functions change in a small quantity way at each iteration step, and the case of zero Lagrange multipliers of the model (21) scarcely occurs at outer iteration steps.

It is assumed that, except the $(l_s-1)\times J+j_s$-th displacement constraint of (22, 23), there exist $(m\text{-}1)$ potential tight constraints in the model (6), which satisfy (24), and they are represented by $g_r^*\left(\boldsymbol{\rho}^{(k-1)}\right),r=2,\cdots,m$. Therefore, when

Table 2 The characteristic data corresponding to the topologies in Fig. 7

Numbering	(a)	(b)	(c)	(d)	(e)	(f)	(g)	(h)
$\|u_{a_y}(\boldsymbol{\rho}^{(k)})\|/\ \|u_{a_y}(\boldsymbol{\rho}^{(0)})\|$	1.036	1.112	1.205	1.382	1.523	1.523	1.523	1.498
$\|u_{q_y}(\boldsymbol{\rho}^{(k)})\|/\ \|u_{q_y}(\boldsymbol{\rho}^{(0)})\|$	1.010	1.077	1.223	1.439	1.518	1.518	1.521	1.496
Volume fraction	0.894	0.788	0.699	0.584	0.523	0.523	0.523	0.527
Black-white fraction	0.957	0.950	0.945	0.940	0.958	0.960	0.960	1.000

Table 3 Constraints and their results obtained by adopting the proposed method for the problem in Fig. 1

Constraints	Final volume fractions	Final displacements	Final topologies
d_a =1.5 , d_q =10.	0.528	$\left\|u_{ay}(\mathbf{\rho}^{opt})\right\|=1.498\left\|u_{ay}(\mathbf{\rho}^{(0)})\right\|$ $\left\|u_{qy}(\mathbf{\rho}^{opt})\right\|=1.321\left\|u_{qy}(\mathbf{\rho}^{(0)})\right\|$	
d_a =1.5 , d_q =1.5	0.527	$\left\|u_{ay}(\mathbf{\rho}^{opt})\right\|=1.495\left\|u_{ay}(\mathbf{\rho}^{(0)})\right\|$ $\left\|u_{qy}(\mathbf{\rho}^{opt})\right\|=1.438\left\|u_{qy}(\mathbf{\rho}^{(0)})\right\|$	
d_a =1.8 , d_q =1.8	0.435	$\left\|u_{ay}(\mathbf{\rho}^{opt})\right\|=1.793\left\|u_{ay}(\mathbf{\rho}^{(0)})\right\|$ $\left\|u_{qy}(\mathbf{\rho}^{opt})\right\|=1.581\left\|u_{qy}(\mathbf{\rho}^{(0)})\right\|$	

Lagrange multipliers of the optimization model (21) all are zeros at the end of the (k-1)-th iteration step, the design element subsets $\mathbf{Q}_1$, $\mathbf{Q}_2$ and $\mathbf{Q}_3$ are easily determined by using the $\left|\partial g^*(\mathbf{\rho}^{(k-1)})/\partial\rho_{n_q}\right|$ of (25). Namely, all int($\delta_1 \times Q$) elements in $\mathbf{Q}_1$ possess the most minimum values of $\left|\partial g^*(\mathbf{\rho}^{(k-1)})/\partial\rho_{n_q}\right|$ within $\mathbf{Q}$, and their topology variables all are bigger than 0.01. And all int($\delta_1 \times Q$) elements in $\mathbf{Q}_2$ possess the most maximum values of $\left|\partial g^*(\mathbf{\rho}^{(k-1)})/\partial\rho_{n_q}\right|$ in (25) within ($\mathbf{Q} - \mathbf{Q}_1$), and their topology variables all are between 0.01 and 0.999 . $\mathbf{Q}_3$ and $\mathbf{Q}_4$ are similarly determined by the approach of Section 3.3.1.

$$\frac{\partial g^*(\mathbf{\rho}^{(k-1)})}{\partial\rho_{n_q}} = \left(\prod_{r=1}^{m} g_r^*(\mathbf{\rho}^{(k-1)})\right)\left(\sum_{r=1}^{m}\frac{\partial g_r^*(\mathbf{\rho}^{(k-1)})\Big/\partial\rho_{n_q}}{g_r^*(\mathbf{\rho}^{(k-1)})}\right) \quad (25)$$

Therefore, the optimization model (6) at the kth iteration step can approximately be transferred into the model (21) by

considering the subsets $\mathbf{Q}_1$, $\mathbf{Q}_2$, $\mathbf{Q}_3$ and $\mathbf{Q}_4$, and (18-20), when Lagrange multipliers of the optimization model (21) all are zeros at the (k-1)-th iteration step.

4 A smooth dual solving method of the approximate problem

Although the optimization model (21) is a linear optimization problem, it is an approximate model of the nonlinear optimization problem (5), and possesses a lot of design variables. If there exist a lot of design variables and only several constraints in an optimization problem, the dual solving method can dramatically reduce the computational quantity (Nocedal and Wright 1999). In order to robustly obtain the solutions of the model (21), following the approach proposed by Svanberg (1987), an artificial variable vector $\mathbf{y} = (y_1, y_2, \cdots, y_{m_\lambda})^T$ is introduced into the problem (21), and $x_q = \rho_{\overline{n}_q}, \overline{n}_q \in \mathbf{Q}_1$, $x_{Q_{red}+q} = \rho_{\tilde{n}_q}, \tilde{n}_q \in \mathbf{Q}_2$ and $x_{Q_{red}+Q_{inc}+q} = \rho_{\underset{\sim}{\tilde{n}_q}}, \overline{\tilde{n}}_q \in \mathbf{Q}_3$ are set at

Table 4 Constraints and their results obtained by Deng and Suresh (2015) for the problem in Fig. 1
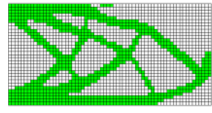
	Constraints	Final volume fractions	Final displacements	Final topologies
(a)	d_a =1.5 , d_q =10.	0.55	$\left\|u_{ay}(\mathbf{\rho}^{opt})\right\|=1.5\left\|u_{ay}(\mathbf{\rho}^{(0)})\right\|$ $\left\|u_{qy}(\mathbf{\rho}^{opt})\right\|=1.63\left\|u_{qy}(\mathbf{\rho}^{(0)})\right\|$	
(b)	d_a =1.5 , d_q =1.5	0.56	$\left\|u_{ay}(\mathbf{\rho}^{opt})\right\|=1.5\left\|u_{ay}(\mathbf{\rho}^{(0)})\right\|$ $\left\|u_{qy}(\mathbf{\rho}^{opt})\right\|=1.4\left\|u_{qy}(\mathbf{\rho}^{(0)})\right\|$	
(c)	d_a =10. , d_q =1.5	0.48	$\left\|u_{ay}(\mathbf{\rho}^{opt})\right\|=1.75\left\|u_{ay}(\mathbf{\rho}^{(0)})\right\|$ $\left\|u_{qy}(\mathbf{\rho}^{opt})\right\|=1.50\left\|u_{qy}(\mathbf{\rho}^{(0)})\right\|$	

Table 5 Two topologies satisfying the allowable constraints (d_a=10. and d_q=1.5.) of the problem in Fig. 1 and their characteristic data

	Topologies	Volume fractions	Displacements
(a)		0.455	$\left\|u_{ay}(\boldsymbol{\rho})\right\|=1.759\left\|u_{ay}(\boldsymbol{\rho}^{(0)})\right\|$ $\left\|u_{qy}(\boldsymbol{\rho})\right\|=1.392\left\|u_{qy}(\boldsymbol{\rho}^{(0)})\right\|$
(b)		0.393	$\left\|u_{ay}(\boldsymbol{\rho})\right\|=2.397\left\|u_{ay}(\boldsymbol{\rho}^{(0)})\right\|$ $\left\|u_{qy}(\boldsymbol{\rho})\right\|=1.423\left\|u_{qy}(\boldsymbol{\rho}^{(0)})\right\|$

each iteration step. The following enlarged approximate problem at the initial point $x_q^{(0)} = \rho_{\bar{n}_q}^{(k-1)}, \bar{n}_q \in \mathbf{Q}_1, x_{Q_{red}+q}^{(0)} = \rho_{\tilde{n}_q}^{(k-1)}$, $\tilde{n}_q \in \mathbf{Q}_2$ and $x_{Q_{red}+Q_{inc}+q}^{(0)} = \rho_{\tilde{\tilde{n}}_q}^{(k-1)}, \tilde{\tilde{n}}_q \in \mathbf{Q}_3$, is given for the displacement constrained optimization problem under multiple load cases.

$$\begin{cases} min \quad f_0(\mathbf{x}) + \sum_{v=1}^{m_\lambda}\left(c_v y_v + \frac{1}{2}d_v y_v^2\right) \\ s.t. \quad g_v(\mathbf{x}) - y_v \leq 0, \quad v = 1, 2, \cdots, m_\lambda \\ \qquad \mathbf{x} \in \mathbf{x}^{(k)}, \quad \mathbf{y} \geq 0 \end{cases} \quad (26)$$

where $m_\lambda = J \times L$

$$f_0(\mathbf{x}) = \left(\sum_{q=1}^{Q_{red}} x_{\bar{n}_q}^{\alpha_v} V_{\bar{n}_q}^0 + \sum_{q=1}^{Q_{inc}} x_{(q+Q_{red})}^{\alpha_v} V_{\tilde{n}_q}^0 + \sum_{q=1}^{Q_{cha}} x_{(q+Q_{red}+Q_{inc})}^{\alpha_v} V_{\tilde{\tilde{n}}_q}^0\right)/V^{(0)}$$

$$g_v(\mathbf{x}) = \left(u_{NC_j}^l(\boldsymbol{\rho}^{(k-1)}) - \tilde{U}_j^{(k)}\right)/\left|u_{NC_j}^{l,(0)}\right| + \sum_{i=1}^{(Q_{red}+Q_{inc}+Q_{cha})}$$

$$\left(\partial\left|u_{NC_j}^l(\boldsymbol{\rho}^{(k-1)})\right|/\partial x_i/\left|u_{NC_j}^{l,(0)}\right|\right)\left(x_i - x_i^{(0)}\right) \quad ,$$

$$v = (l-1) \times J + j, \quad j = 1, 2, \cdots, J; l = 1, 2, \cdots, L \quad (27)$$

$$\mathbf{x}^{(k)} = \left\{x_i | x_i \in \left[x_i^L, x_i^U\right], \quad i = 1, 2, \cdots, (Q_{red} + Q_{inc} + Q_{cha})\right\} \quad (28)$$

Being referred to the paper published by Svanberg (1987), $c_1 = 1000$ and $d_1 = 1.0$ are selected in the examples of this paper. At the beginning of the sub-optimization iterations, it is necessary to choose $\mathbf{x}^{(0)}$, and then to compute $\mathbf{y}^{(0)}$, and obtain an initial feasible estimate $(\mathbf{x}^{(0)}, \mathbf{y}^{(0)})^T$ of the problem (26). Considering only the main constraints, since the simple box and the non-negativity constraints of the artificial variables $\mathbf{y} = (y_1, y_2, \cdots, y_{m_\lambda})^T$ will be incorporated in the minimization process, the Lagrange function corresponding to the problem (19) may be given by

$$\tilde{L}(\mathbf{x}, \lambda) = f_0(\mathbf{x}) + \sum_{v=1}^{m_\lambda}\lambda_v(g_v(\mathbf{x}) - y_v) + \sum_{v=1}^{m_\lambda}\left(c_v y_v + \frac{1}{2}d_v y_v^2\right) \quad (29)$$

The programming problem (26) can be transferred into following dual programming problem by the dual theory.

$$\begin{aligned} max: \quad &\phi(\lambda) \\ s.t. \quad &\lambda \geq 0.0 \end{aligned} \quad (30)$$

where, $\phi(\lambda) = \min_{\mathbf{x}, \mathbf{y}}\left\{\tilde{L}(\mathbf{x}, \mathbf{y}, \lambda), x_i \in [x_i^L, x_i^U], \mathbf{y} \geq 0\right\}$.

To obtain an iteration solution of (26) by adopting an iteration solution of Lagrange multipliers in the model (30), the function relations of the design variables with respect to the Lagrange multiplier vector must approximately be given. Based on the KKT condition (Nocedal and Wright 1999), following equation may be gotten.

$$\frac{\partial\tilde{L}(\mathbf{x}, \lambda)}{\partial x_i} = \frac{\partial f_0(\mathbf{x})}{\partial x_i} + \sum_{v=1}^{m_\lambda}\lambda_v\frac{\partial g_v(\mathbf{x})}{\partial x_i} = 0.0, \quad i$$
$$= 1, 2, \cdots, (Q_{red} + Q_{inc} + Q_{cha}) \quad (31)$$

Fig. 9 The load case and the support condition of a MBB beam, and an initial structural model for its analysis and optimization

$E=1, v=0.3, F=1, l=6, h=1, \bar{V}=0.34$
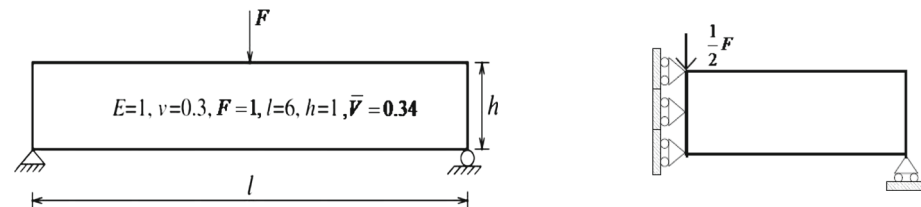
(a) A MBB beam (unit thickness; plane stress)

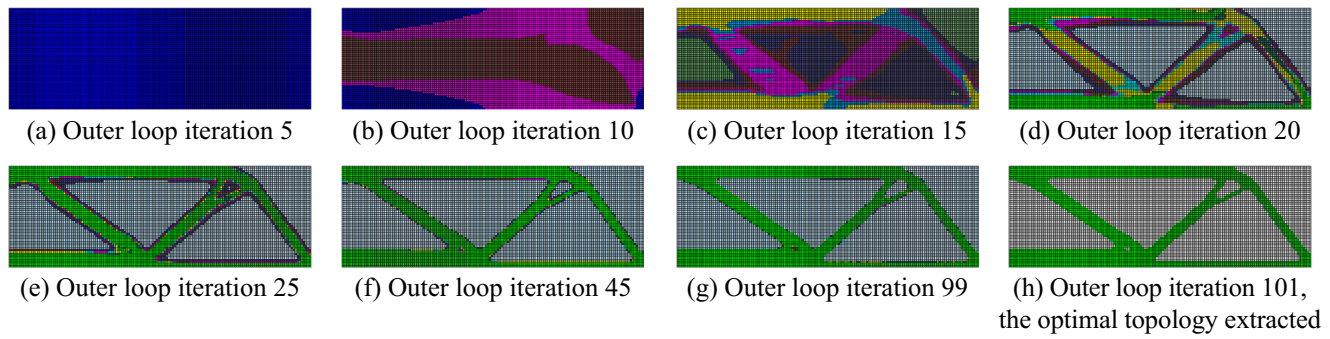(b) half design domain and its initial structural model

Fig. 10 The topology distribution optimization history of the half MBB beam, which is obtained by using the SIMP method for the initial structural model with topology variables all being 0.8

Multiplying (31) by $x_i^{(r)}(\boldsymbol{\lambda})$, following equation can be obtained.

$$-\frac{\sum_{v=1}^{m_\lambda} \lambda_v \frac{\partial g_v(\mathbf{x})}{\partial x_i}}{\frac{\partial f_0(\mathbf{x})}{\partial x_i}} = -\frac{\sum_{v=1}^{m_\lambda} \lambda_v \frac{\partial g_v(\mathbf{x})}{\partial x_i} x_i^{(r)}(\boldsymbol{\lambda})}{\frac{\partial f_0(\mathbf{x})}{\partial x_i} x_i^{(r)}(\boldsymbol{\lambda})} = 1 \ , \quad (32)$$

$$i = 1, 2, \cdots, (Q_{red} + Q_{inc} + Q_{cha})$$

where $x_i^{(r)}(\boldsymbol{\lambda})$ denotes the ith design variable at the kth outer iteration and the rth sub-iteration.

From (32), an iteration formula can be built as follows:

$$x_i^{*(r+1)}(\boldsymbol{\lambda}) = -\frac{\sum_{v=1}^{m_\lambda} \lambda_v \frac{\partial g_v(\mathbf{x}^{(0)})}{\partial x_i}}{\frac{\partial f_0(\mathbf{x}^{(0)})}{\partial x_i}} x_i^{(r)}(\boldsymbol{\lambda}) \quad (33)$$

where $x_i^{*(r+1)}(\boldsymbol{\lambda})$ denotes the ith design variable obtained by using the KKT condition at the kth outer iteration and the

$(r+1)$-th sub-iteration, and $\mathbf{x}^{(0)}$ denotes the design variable vector at the beginning sub-iteration of the kth outer iteration.

A so-called fixed point iteration method has widely been used in solving the roots of a nonlinear equation. In order to ensure iteration convergence, a scalar relaxation parameter γ(Burden and Faires 1985; Du and Taylor 2002) is introduced into (33), and the (33) becomes

$$x_i^{*(r+1)}(\boldsymbol{\lambda}) = \gamma \frac{-\sum_{v=1}^{m_\lambda} \lambda_v \frac{\partial g_v(\mathbf{x}^{(0)})}{\partial x_i}}{\frac{\partial f_0(\mathbf{x}^{(0)})}{\partial x_i}} x_i^{(r)}(\boldsymbol{\lambda}) + (1-\gamma) x_i^{(r)}(\boldsymbol{\lambda}) \quad (34)$$

Really, the change quantities of design variables can be appropriately adjusted by a change of γ, and γ will affect all design variables and ensure iteration convergence. And a value of $[0.02, 0.12]$ is selected as γ in the examples of Burden and Faires (1985)and Du and Taylor (2002) and this paper. From (34), following equation may be derived

$$\frac{\partial x_i^{*(r+1)}(\boldsymbol{\lambda})}{\partial \lambda_v} = -\gamma \left(\frac{\partial g_v(\mathbf{x}^{(0)})/\partial x_i}{\partial f_0(\mathbf{x}^{(0)})/\partial x_i} \right) x_i^{(r)}(\boldsymbol{\lambda}) \quad (35)$$

Considering the upper and lower limits of the design variables, the design variable $x_i^{(r+1)}(\boldsymbol{\lambda})$ and the artificial variable $y_v^{(r+1)}(\boldsymbol{\lambda})$ can be calculated by

$$x_i^{(r+1)}(\boldsymbol{\lambda}) = \max\left\{ x_i^L, \min\left\{ x_i^U, x_i^{*(r+1)}(\boldsymbol{\lambda}) \right\} \right\}, \quad i$$
$$= 1, 2, \cdots, (Q_{red} + Q_{inc} + Q_{cha}) \quad (36)$$

$$y_v^{(r+1)}(\lambda_v) = \max\left(0.0, \ \frac{\lambda_v - c_v}{d_v} \right), \quad v = 1, 2, \cdots, m_\lambda \quad (37)$$

Note that $x_i^{(r+1)}(\boldsymbol{\lambda}) : R^{m_\lambda} \rightarrow R$ and $y_v^{(r+1)}(\lambda_v) : R \rightarrow R$ are continuous functions of the Lagrange multiplier vector $\boldsymbol{\lambda}$, but not differentiable at the point $\boldsymbol{\lambda}$ that $x_i^{(r+1)}(\boldsymbol{\lambda}) = x_i^L$ or $x_i^{(r+1)}(\boldsymbol{\lambda}) = x_i^U$ for $i = 1, 2, \cdots, (Q_{red} + Q_{inc} + Q_{cha})$ and $\lambda_v = c_v$ for $v = 1, 2, \cdots, m_\lambda$.
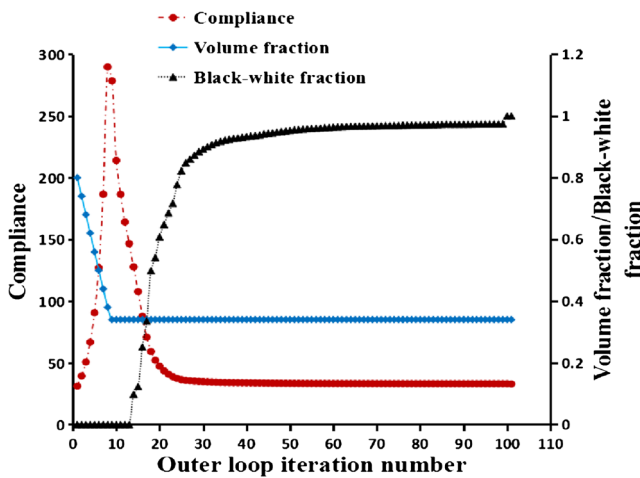

Fig. 11 The volume fraction, black and white fraction and total compliance optimization histories of the half MBB beam, which are obtained by using the SIMP method for the initial structural model with topology variables all being 0.8

Table 6 The characteristic data corresponding to the topologies in Fig.10

Numbering	(a)	(b)	(c)	(d)	(e)	(f)	(g)	(h)
Total compliance	127.13	186.50	87.788	43.474	35.668	33.457	33.019	32.804
Volume	1.5000	1.0200	1.0200	1.0200	1.0200	1.0200	1.0200	1.0201
Black-white fraction	0.0000	0.0000	0.2509	0.6469	0.8479	0.9451	0.9743	1.0000
Displacement	508.51	746.02	351.15	173.89	142.67	133.83	132.08	131.29

Rong et al. (2016) investigated continuum structural topological optimization with stress constraints based on an active constraint technique and reciprocal topology variables. In the method, a strategy with two optimization phases and a phase transferring step, and a smooth dual solving approach were proposed to heuristically remove a lot of elements with topology variables between 0.15 and 0.001 at some iterations. Here, the smooth dual solving method proposed by Rong et al. (2016) is adopted to solve the approximate sub-problem. $x_i^{(r+1)}(\boldsymbol{\lambda})$ and $y_v^{(r+1)}(\lambda_v)$ in (36) and (37) may be approximately transformed into the following smoothing functions $\tilde{x}_i^{(r+1)}(\boldsymbol{\lambda})$ and $\tilde{y}_v^{(r+1)}(\lambda_v)$.

$$\tilde{x}_i^{(r+1)}(\boldsymbol{\lambda}) = x_i^L + p_1 \ln\left(1 + e^{z_i^{(r+1)}(\boldsymbol{\lambda})/p_1}\right), \quad i$$
$$= 1, 2, \cdots, (Q_{red} + Q_{inc} + Q_{cha}) \tag{38}$$

$$\tilde{y}_v^{(r+1)}(\lambda_v) = p_1 \ln\left(1 + e^{(\lambda_v - c_v)/(p_1 d_v)}\right), \quad v$$
$$= 1, 2, \cdots, m_\lambda \tag{39}$$

where $z_i^{(r+1)}(\boldsymbol{\lambda}) = \left(x_i^U - x_i^L\right) - p_2 \ln\left(1 + e^{\left(-x_i^{*(r+1)}(\boldsymbol{\lambda}) + x_i^U\right)p_2}\right)$, p_1 and p_2 are two small positive parameters. At the rth sub-iteration step, the p_1 and p_2 of the (38, 39) are replaced by $p_1^{(r)}$ and $p_2^{(r)}$.

Therefore, an approximate quadratic programming model of the dual programming problem (30) can easily be obtained by adopting (29, 30, 34–39), combining the approach of Section 4.2 in Rong et al. (2016). And the detail approach of the approximate quadratic programming model and its simple solving approach are referred to Section 4.2 of the paper published by Rong et al. (2016).

5 A filtering scheme and a stabilization of the optimization process

To circumvent numerical instabilities, such as checkerboard patterns and mesh-dependency, a sensitivity filtering scheme being similar to that of Sigmund and Peterson (1998), is adopted. The defined filtering function is based on a filtering length scale $r_{\min}$ that does not change with its mesh refinement. A circle of a radius $r_{\min}$, centered at the centroid of the eth element, and the circular sub-domain $\overline{\Omega}_e$ may be generated. Elements, whose centroids are located inside $\overline{\Omega}_e$, contribute to the computation of the improved sensitivity of the eth element as

$$\partial \left|\overline{u}_{NC_j}^l\left(\boldsymbol{\rho}^{(k-1)}\right)\right| \Big/ \partial \rho_e$$
$$= \frac{\sum\limits_{q=1}^{Q} w\left(r_{e\,n_q}\right)\left(\rho_{n_q}^{(k-1)}\right)^\alpha \partial \left|u_{NC_j}^l\left(\boldsymbol{\rho}^{(k-1)}\right)\right| \Big/ \partial \rho_{n_q}}{\left(\rho_e^{(k-1)}\right)^\alpha \sum\limits_{q=1}^{Q} w\left(r_{e\,n_q}\right)},$$
$$e \in \mathbf{Q}; \quad j = 1, 2, \cdots, J; l = 1, 2, \cdots, L \tag{40}$$

(a) Outer loop iteration 5   (b) Outer loop iteration 10   (c) Outer loop iteration 15   (d) Outer loop iteration 20

(e) Outer loop iteration 25   (f) Outer loop iteration 45   (g) Outer loop iteration 99   (h) Outer loop iteration 101, the optimal topology extracted
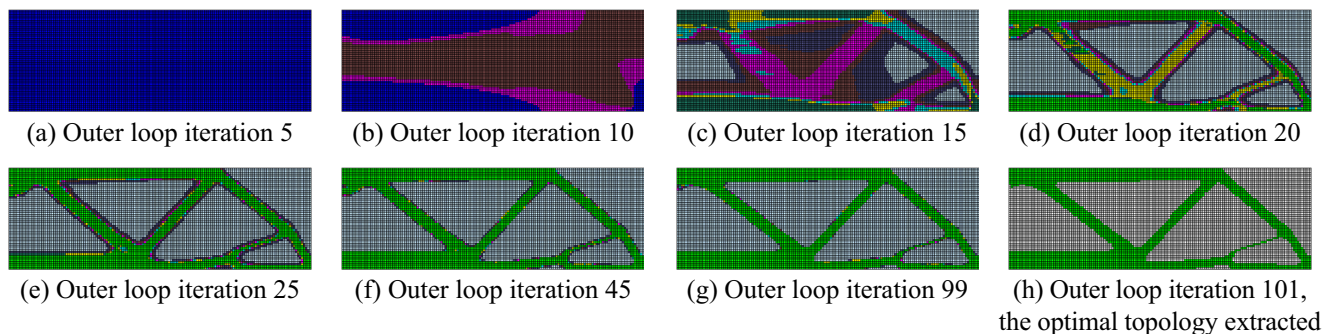
Fig. 12 The topology distribution optimization history of the half MBB beam, which is obtained by using the SIMP method for the initial structural model with topology variables all being 1.0
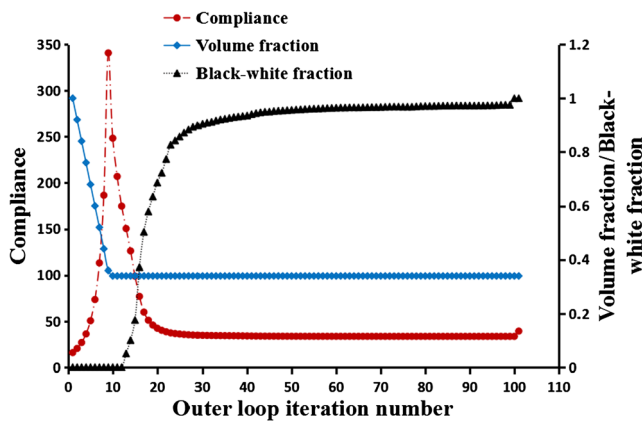
Fig. 13 The volume fraction, black and white fraction and total compliance optimization histories of the half MBB beam, obtained by using the SIMP method for the initial structural model with topology variables all being 1.0

The convolution operator (weight factor) $w\left(r_{e\,n_q}\right)$ is written as

$$w\left(r_{e\,n_q}\right) = \begin{cases} r_{\min} - r_{e\,n_q}, & r_{e\,n_q} < r_{\min} \\ 0.0, & r_{e\,n_q} \geq r_{\min} \end{cases} \tag{41}$$

where $r_{e\,n_q}$ is the distance between the centre of the eth element and the centre of the n_q-th element, and the value selection of $r_{e\,n_q}$ is discussed in many references (Sigmund 2001, Wood and Groenwold 2010 and etc.). α of (40) is an empirical parameter, and its value is between 0.15 and 0.25. To further improve the sensitivity accuracy, the simple way provided by Huang and Xie (2007) is adopted, and its formula is expressed as:

$$\partial\left|u_{NC_j}^l\left(\boldsymbol{\rho}^{(k-1)}\right)\right|\Big/\partial\rho_e = (1-\chi_s)\partial\left|\overline{u}_{NC_j}^l\left(\boldsymbol{\rho}^{(k-2)}\right)\right|\Big/\partial\rho_e$$
$$+ \chi_s\partial\left|\overline{u}_{NC_j}^l\left(\boldsymbol{\rho}^{(k-1)}\right)\right|\Big/\partial\rho_e, \quad e\in\mathbf{Q} \tag{42}$$

Then, $\partial\left|u_{NC_j}^l\left(\boldsymbol{\rho}^{(k-1)}\right)\right|\big/\partial\rho_e$ in (15,16) and (27) is replaced by $\partial\left|u_{NC_j}^l\left(\boldsymbol{\rho}^{(k-1)}\right)\right|\big/\partial\rho_e$ in (42). χ_s is another empirical parameter, and 0.7 is selected as its value in examples of this paper according to the suggestion of Huang and Xie (2007).

6 A stopping iteration criterion and a black and white fraction

The outer loop finishes successfully whenever the following two conditions all are satisfied.

$$\min_{j=1,2,\cdots,J;\;\;l=1,2,\cdots,L}\left\{\left(U_j - \left|u_{NC_j}^l\left(\boldsymbol{\rho}^{(k)}\right)\right|\right)\Big/U_j\right\} \leq \varepsilon_1 \tag{43}$$

$$\left|\left(V^{(k)} - \frac{V^{(k-1)} + V^{(k-2)}}{2}\right)\Big/V^{(k)}\right| \leq \varepsilon_1 \tag{44}$$

where, ε_1 is an allowable small convergence parameter. $\varepsilon_1 = 0.001$ often was adopted in examples of papers published by many authors, such as Huang and Xie (2007), Xia et al. (2012) and Zuo and Xie (2014), and also is adopted in the examples of this paper.

Similarly, the elemental 'black and white fraction $\varphi_{B\,\&\,W}$' in Groenwold et al. (2009) and Wood and Groenwold (2010), is adopted. Its expression is given as follows:

$$\varphi_{B\&W} = \left(N_{[0]} + N_{[1]}\right)\Big/N \tag{45}$$

where $N_{[0]}$ and $N_{[1]}$, respectively, represent the element number of the subset $\{\,i\;|\rho_i \leq 0.001\,\}$, and the element number of the subset $\{\,i\;|\rho_i \geq 0.999\,\}$. And N denotes the total number of the structural elements in the fixed design domain.

7 Numerical examples

7.1 Optimization designs of the classic 2-D cantilever beam

Two displacement constraints in Fig. 1 (Deng and Suresh 2015) are imposed: one at the point of force application, and the other at a point of interest 'q' located in the middle of the top edge in Fig. 1:

$$\left|u_{ay}(\boldsymbol{\rho})\right| - d_a\left|u_{ay}\left(\boldsymbol{\rho}^{(0)}\right)\right| \leq 0$$
$$\left|u_{qy}(\boldsymbol{\rho})\right| - d_q\left|u_{qy}\left(\boldsymbol{\rho}^{(0)}\right)\right| \leq 0 \tag{46}$$

Here, the filtering length scale $r_{\min} = 2\Delta_{\min} = 0.01m$ ($\Delta_{\min}$ is the minimum side length of all structural elements) being the same as that of Deng and Suresh (2015), is adopted. And

Table 7 The characteristic data corresponding to the topologies in Fig.12

Numbering	(a)	(b)	(c)	(d)	(e)	(f)	(g)	(h)
Total compliance	73.569	207.05	76.989	40.089	35.629	33.708	33.497	39.235
Volume	1.8000	1.0200	1.0200	1.0200	1.0200	1.0200	1.0200	1.0196
Black-white fraction	0.000	0.000	0.3721	0.7232	0.8717	0.9521	0.9753	1.0000
Displacement	294.28	828.20	307.96	160.35	142.52	134.83	133.99	156.94

(a) Outer loop iteration 5   (b) Outer loop iteration 10   (c) Outer loop iteration 15   (d) Outer loop iteration 20

(e) Outer loop iteration 25   (f) Outer loop iteration 45   (g) Outer loop iteration 95   (h) Outer loop iteration 97, the optimal topology extracted
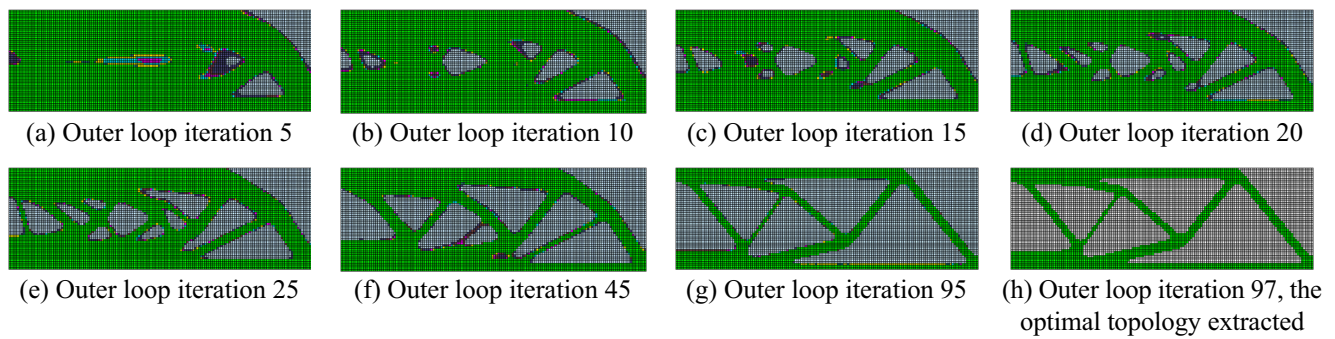
Fig. 14 The topology distribution optimization history of the half MBB beam, which is obtained by using the proposed method for the initial structural model with topology variables all being 1.0

the empirical parameters β_1=0.004, $\delta_1 = 0.1$, and γ=0.1 are adopted. Other five parameters are selected according to the suggestion values in corresponding sections of this paper. Here, the empirical parameters δ_1, γ and β_1 are treated as important empirical parameters, and are determined according to a small change principle of structural characteristic quantities. Really, β_1 is the most active and important empirical parameter. δ_1 means that the topology variables of only certain number elements are allowed to change within a large range at each iteration step. γ and β_1 mean that certain change quantities of design variables are allowed, and β_1 is a total control quantity of design variable changes. When small values of γ and β_1 are given, the quantity of δ_1 will affect the gray distribution and its optimization iteration numbers. A small value of δ_1 will lead to very good black/white distributions and many iteration numbers required. A big value of δ_1 will lead to poor black/white distributions. The empirical parameter value δ_1 is easily determined by a trial calculation and a black/white distribution requirement. A lot of simulations demonstrate that if a value of [0.003,0.012] is adopted as δ_1, a series of topologies with good black/white distributions and convergence, can be guaranteed before about 120 iteration steps. The empirical parameter values γ and β_1 are easily determined by a trial calculation and the requirement of at least one non-zero Lagrange multiplier of the approximate model at most iteration steps for any example. γ and β_1 must be increased before structural optimization when the optimization solution needs too many iteration numbers. And γ and β_1 must be reduced before structural optimization when there exist some bad topological configurations during an optimization process. A value of [0.03, 0.12] may be selected as γ, and a value of [0.002, 0.008] may be selected as β_1.

Figure 5 gives the topology distribution optimization history of the cantilever beam, which is obtained by adopting the proposed method for the allowable constraint parameters d_a=1.5 and d_q=1.5, and the volume penalty parameter α_v=1.0, when topology variables of the initial structural model all are 1. Fig. 6 gives the volume fraction, the black and white fraction and displacement ratio optimization histories of the cantilever beam, corresponding to Fig. 5. The structural

topology characteristic data in Fig. 5, are given in Table 1. Its computational time employed by adopting the computer with CPU 2.66G is 283s.

It is seen from Fig. 5 that although the topologies obtained at all iterative steps include gray elements, the number of the elements whose topology variables are below 0.001, increases with an increase in outer iteration number; and there only are a few of the gray elements, whose topology variables are between 0.001 and 0.95. It is found from its optimization process that at least one displacement constraint is an active constraint at almost all iteration steps. Fig. 6 and the Table 1 also show that black and white fractions of all topologies are bigger than 0.85. Fig. 6 shows that constraint displacements and the structural volume stably and smoothly change, and the black and white fraction changes in a way of very small fluctuations during the optimization process.

If the volume penalty parameter α_v=0.8 and the previous other conditions are adopted, optimization results obtained by using the proposed method are shown in Fig. 7, Fig. 8 and Table 2. Fig. 7, Fig. 8 and Table 2 show that a series of topologies obtained, possess a more predominant black-and-white distribution than topologies in Fig. 5. Fig. 7 also depicts that
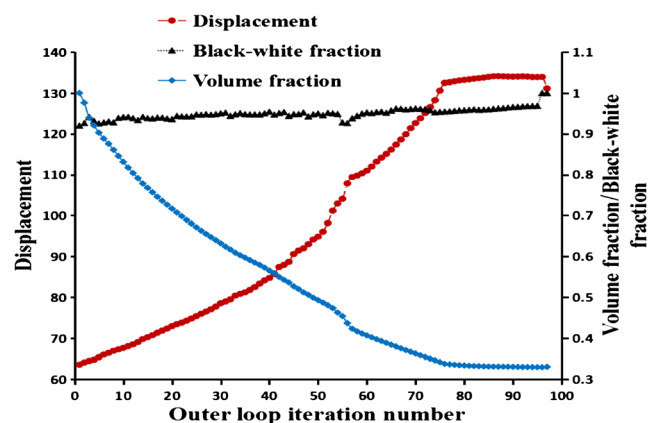

Fig. 15 The volume fraction, black and white fraction and total compliance optimization histories of the half MBB beam, obtained by using the proposed method for the initial structural model with topology variables all being 1.0

Table 8 The characteristic data corresponding to the topologies in Fig.16

Numbering	(a)	(b)	(c)	(d)	(e)	(f)	(g)	(h)
Displacement	66.004	68.044	70.722	73.418	75.977	91.448	133.827	131.12
Volume	2.6648	2.4510	2.2701	2.1217	1.9895	1.5606	0.9881	0.9906
Black-white fraction	0.9276	0.9415	0.9375	0.9439	0.9467	0.9484	0.9685	1.0000
Total compliance	16.501	17.011	17.681	18.355	18.994	22.862	33.457	32.730

the results obtained after several iterations provide a series of topologies with clear profiles.

If the volume penalty parameter α_v=0.8 and the aforementioned other empirical parameter values are adopted, the results obtained by using the proposed method for the problem in Fig. 1 and corresponding different values for the allowable relative displacements at both constraint points of interest, are listed in Table 3. Table 4 gives constraints and relative results obtained by Deng and Suresh (2015) for the problem. Comparing Table 3 and Table 4, it is concluded that two more optimal topologies with different configurations and more 4.5% reductions of the objective function than the results of the Deng and Suresh method (2015), are obtained by using the proposed method for this example with the allowable relative parameters d_a=1.5 and d_q=10., and d_a=1.5, and d_q=1.5, respectively .

For the allowable relative parameters d_a=10. and d_q=1.5., although the convergent optimal solution of the problem in Fig. 1 is not obtained by adopting the proposed method, two topologies satisfying the allowable constraints (d_a=10. and d_q=1.5.) of the problem in Fig. 1, are obtained by use of the proposed method, and are shown in Table 5. Comparing Table 3, Table 4 and Table 5, it is concluded that the proposed method can obtain a more optimal topology than the Deng and Suresh method (2015) for a reasonable displacement constraint model of Fig. 1. Table 5 (b) also shows that although the topology with a bigger volume reduction, satisfies the allowable constraints (d_a=10. and d_q=1.5.) of the problem in Fig. 1, the constraint displacement point q is disconnected from the support. Therefore, there exists a reasonable displacement constraint modeling problem or a disconnected constraint point problem in the proposed method. In view of the fact that the topology of Table 5(a) possesses a smaller volume than that of Table 4 (c), a reasonable displacement constraint modeling problem or a disconnected constraint point problem (which is similar to an ill load optimization problem) will be a problem to be investigated.

7.2 A classic MBB beam design subjected to one concentrated load

To further estimate the proposed method, the SIMP method (Sigmund 2001) combined with the simple heuristic approach for the gray-scale suppression (Groenwold et al. 2009), is programmed in Fortran. And the compliance minimization

problem of the well-known MBB beam in Fig. 9 with a volume ratio limit 0.34 is solved by the SIMP method Fortran code to obtain the vertical displacement value at the loading point and the optimum topological configuration. Here, the SIMP penalty parameter p=3 and the gray-scale suppression parameter q=2 (Groenwold et al. 2009), a move limit parameter 0.1 and a convergence error 0.001 are adopted. Then, the vertical displacement value at the loading point of the optimum topology is taken as a displacement constraint value of the proposed model, and the MBB beam design is solved by the proposed method.

Considering the symmetries of the structure and the load, only half design domain in Fig. 9b is to be optimized. And the problem settings are as follows: a finite element mesh model with 150×50 equal-size four-node plane stress elements and a linear sensitivity filter with radius $r_{\min} = 4\Delta_{\min} = 0.08$ are adopted.

The topology variable distribution optimization history of the half MBB structure is presented in Fig. 10, which is obtained by adopting the SIMP method (Groenwold et al. 2009) for the initial structural model with topology variables all being 0.8. Fig. 11 gives the volume fraction, black and white fraction and total compliance optimization histories of the half MBB beam. Numerical characteristic results corresponding to the topologies in Fig. 10, are presented in the Table 6. Its computational time employed by adopting the computer with CPU 2.66G is 1455s. It is found from Fig. 10 and Fig. 11 that there exist some big jumps in the compliance at the beginning iteration steps.

The results of the half MBB beam optimization are presented in Fig. 12, Fig. 13 and Table 7, which are obtained by adopting the SIMP method when topology variables of the initial structural model all are 1. Here, all empirical parameter values are the same as that adopted in Fig. 10. Fig. 10h and Fig. 12h show that the SIMP method can obtain an optimal topology with a predominantly black-and-white distribution
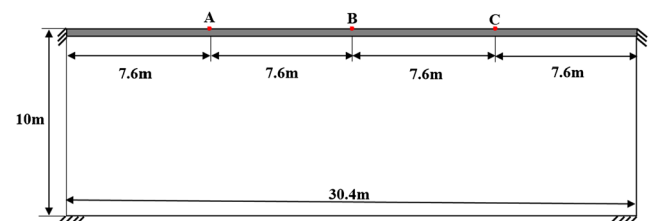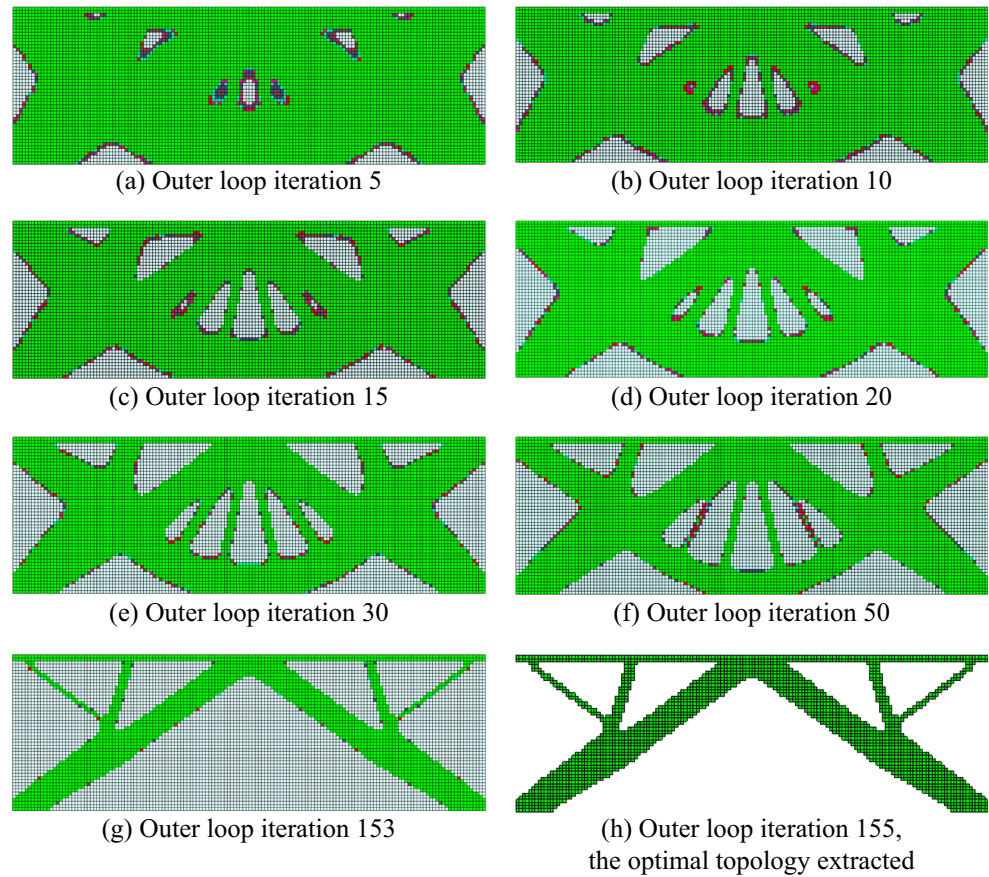

Fig. 16 The initial structural model of an arch structure

Fig. 17 The topology distribution optimization history of an arch bridge structure, which is obtained by using the proposed method

(a) Outer loop iteration 5

(b) Outer loop iteration 10

(c) Outer loop iteration 15

(d) Outer loop iteration 20

(e) Outer loop iteration 30

(f) Outer loop iteration 50

(g) Outer loop iteration 153

(h) Outer loop iteration 155, the optimal topology extracted

for each of two different initial topologies, but the optimal topology obtained by adopting the SIMP method for the initial topology with topology variables all being 1.0, possesses one-point hinge connection elements and a bigger compliance.

Here, the displacement value 131.30 abstracted from Fig. 10h and Table 6(h), is taken as a displacement constraint value of the proposed model for Fig. 9. Here, $r_{min} = 4\Delta_{min} = 0.08$ being the same as that of the SIMP method, and empirical parameters $\beta_1 = 0.003$, $\delta_1 = 0.08$ and $\gamma = 0.05$ are adopted. The results of the half MBB beam optimization are presented in Fig. 14, Fig. 15 and Table 8, which are obtained by adopting the proposed method when topology variables of the initial structural model all are 1.0. It is seen from Fig. 15 that the black and white fraction, the volume fraction and the con-straint displacement stably and smoothly change with an in-crease in outer iteration number. It is found from Fig. 10h, Table 6, Fig. 14h and Table 8h that the proposed method can obtain an optimal topology with a smaller volume and a basic same black and white fraction than the SIMP method for the same vertical displacement of the applied load point.

7.3 An arch bridge example under multiple load cases

Figure 16 shows the two-dimensional design domain of an arch bridge, where the most left and most right sides in the

range of 0.6 m at the bottom of the bridge, and the upper ends in the range of 0.4 m at its left hand and right hand sides, respectively, are fixed. A uniform distributed load of $\rho_1 = 30kN/m$ is acting on the top side of a non-designable deck layer (its thickness is 0.4 m) of the bridge. And another load case with a uniform distributed load of $\rho_2 = 460kN/m$ being applied on the partial top side with a 0.8 m interval centered at point A of the bridge top, is considered. Here, points A, B and C are uniformly distributed at the top side of the bridge. And the third load case with three same uniform distributed loads of $\rho_3 = 270kN/m$ being applied on three partial top sides with three same 0.8 m intervals centered at points A, B and C of the bridge, respectively, is given. The gravity load is not
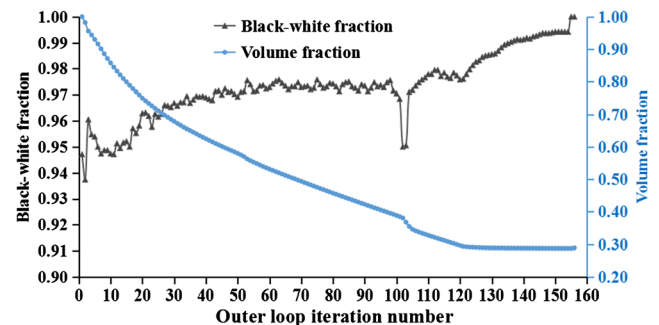

Fig. 18 The volume fraction and black-white fraction histories of the bridge structure, obtained by using the proposed method

Table 9 The constraint direction displacement data of the initial and final topologies

	The initial structural displacements			The final structural displacements		
Constraint point **numbering**	A	B	C	A	B	C
Displacements of load case 1 / um	3.954	5.390	3.954	14.78	14.05	14.78
Displacements of load case 2 / um	2.115	5.186	2.115	3.968	14.91	3.968
Displacements of load case 3 / um	4.144	5.527	4.144	14.86	13.47	14.86

considered in the structural analyses and optimization. The bridge is assumed to be constructed by reinforced concrete. The Young's modules $E^0 = 4.25 MPa$ and Poisson's ratio $\nu = 0.2$ are specified in the analyses.

The structural maximum domain is modeled by adopting a finite element mesh model with 152×50 equal-size four-node plane strain elements, its two-dimension size is 30.4m × 10m, and its thickness is 10m. And a linear sensitivity filter with radius $r_{min} = 4\Delta_{min} = 0.8m$ is adopted. The thickness of the bridge desk is 0.4m and the bridge desk is defined as a non-design domain.

A prescribed displacement 14.9um is taken as the vertical displacement constraint values of A, B and C points under the three load cases for the model (5) of Fig. 16. Here, empirical parameters β_1=0.003, $\delta_1 = 0.06$ and γ=0.04 are adopted. The results of the bridge optimization are presented in Fig. 17 and Fig.18, which are obtained by the proposed method when topology variables of the initial structural model all are 1. The initial and final structural volumes are 3040m^3 and 877.0m^3, respectively. Table 9 gives the constraint direction displacement data of the initial and final topologies. Fig. 18 shows that the black and white fraction changes in a way of fluctuations during the optimization process. When components disappear at some iteration steps (Fig. 17), there are several big jumps in the black and white fraction curve of Fig. 18. The aforementioned good feature can be found in Figs.17-19.

8 Conclusions

A novel displacement constrained optimization approach for black and white structural topology designs under multiple load cases, is proposed. Some examples are given to demonstrate that the feasibility and effectiveness and features of the proposed method. The following conclusions can be drawn:

(1) Two improved schemes dealing with trust regions and adjustments of constraint limits, respectively, are proposed. The proposed approximate optimization model possesses a tight constraint feature and can approximately adhere to the binary change nature requirement of structural topology optimization.

(2) An improved optimization method for a displacement constrained topology optimization problem is proposed, which possesses convergence and the robustness of the optimization process.

(3) The proposed method can obtain an optimal topology with a predominantly black-and-white distribution, and a series of topologies with clear profiles during an optimization process for the topology optimization problem under multiple load cases.

(4) The disconnected constraint point problem and the solid/empty solving issue of topology optimization with more structural behavior constraints under multiple load

Fig. 19 The vertical displacement optimization histories of the bridge constraint points, obtained by using the proposed method
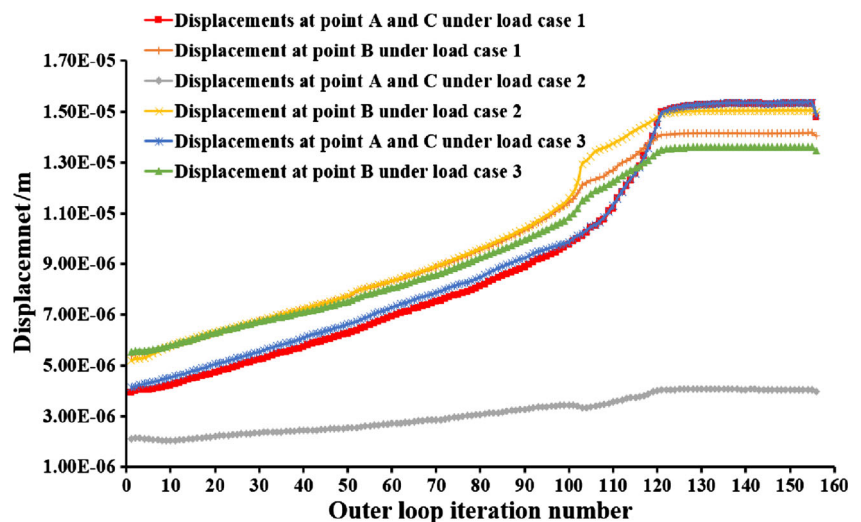
cases, require further mathematical and scientific developments.

References

Bruns TE (2005) A reevaluation of the SIMP method with filtering and an alternative formulation for solid-void topology optimization. Struct. Multidisc. Optim. 30:428–436

Burden R, Faires J (1985) Numerical analysis, 3rd edn. Prindle, Weber and Schmidt, Boston

Deaton JD, Grandhi RV (2014) A survey of structural and multidisciplinary continuum topology optimization: post 2000. Struct. Multidisc. Optim. 49:1–38

Deng S, Suresh K (2015) Multi-constrained topology optimization via the topological sensitivity. Struct. Multidisc. Optim. 51:987–1001

Du J, Taylor JE (2002) Application of an energy-based model for the optimal design of structural materials and topology. Struct. Multidisc. Optim. 24:277–292

Fleury C (1989) Efficient approximation concepts using second order information. Int. J. Numer. Meth. Eng. 28:2041–2058

Fuchs MB, Jiny S, Peleg N (2005) The SRV constraint for 0/1 topological design. Struct. Multidisc. Optim. 30:320–326

Fujii D, Kikuchi N (2000) Improvement of numerical instabilities in topology optimization using the SLP method. Struct Multidisc Optim 19:113–121

Garcia-Lopez NP, Sanchez-Silva M, Medaglia AL, Chateauneuf A (2011) A hybrid topology optimization methodology combining simulated annealing and SIMP. Comput Struct 89:1512–1522

Groenwold AA, Etman LFP (2009) A simple heuristic for gray-scale suppression in optimality criterion-based topology optimization. Struct. Multidisc. Optim. 39:217–225

Groenwold AA, Wood DW, Etman LFP, Tosserams S (2009) Globally convergent optimization algorithm using conservative convex separable diagonal quadratic approximations. AIAA J 47:2649–2657

Guedes JM, Taylor JE (1997) On the prediction of material properties and topology for optimal continuum structures. Struct. Optim. 14:193–199

Guest JK, Prevost JH, Belytschko T (2004) Achieving minimum length scale in topology optimization using nodal design variables and projection functions. Int. J. Numer. Meth. Eng. 61(2):238–254

Haber RB (1996) A new approach to variable-topology shape design using a constraint on perimeter. Struct. Optim. 11:1–12

Huang X, Xie YM (2007) Convergent and mesh-independent solutions for the bi-directional evolutionary structural optimization method. Finite Elem Anal Des 43(14):1039–1049

Huang X, Xie YM (2010) Evolutionary topology optimization of continuum structures with an additional displacement constraint. Struct Multidiscip Optim 40:409–416

Jang GW, Kim MJ, Kim YY (2009) Design optimization of compliant mechanisms consisting of standardized elements. ASME Journal of Mechanical Design 131:121006

Kikuchi N, Nishiwaki S, Fonseca JSO, Silva ECN (1998) Design optimization method for compliant mechanisms and material microstructure. Comput Methods Appl Mech Eng 151:401–417

Liang QQ, Xie YM, Steven GP (2001) A performance index for topology and shape optimization of plate bending problems with displacement constraints. Struct Multidiscip Optim 21:393–399

Liu XJ, Li ZD, Chen X (2011) A new solution for topology optimization problems with multiple loads: the guide-weight method. Sci China Tech Sci 54:1505–1514

Nocedal J, Wright SJ (1999) Numerical Optimization. Springer, New York

Olhoff N, Bendsøe MP, Rasmussen J (1991) On CAD-integrated structural topology and design optimization. Comput Methods Appl Mech Eng 89:259–279

Petersson J, Sigmund O (1998) Slope constrained topology optimization. Int. J. Numer. Meth. Eng. 41:1417–1434

Rietz A (2001) Sufficiency of a finite exponent in SIMP (power law) methods. Struct Multidiscip Optim 21:159–163

Rong JH, Yi JH (2010) A structural topological optimization method for multi-displacement constraint problems and any initial topology configuration. International Journal of Acta Mechanica Sinica 26:735–744

Rong JH, Liu XH, Yi JJ (2011) An efficient structural topological optimization method for continuum structures with multiple displacement constraints. International Journal of Finite Elements in Analysis and Design 47:913–921

Rong JH, Xiao TT, Yu LH et al (2016) Continuum structural topological optimization with stress constraints based on an active constraint technique. Int J Numer Meth Eng 108(4):326–360

Sauter M, Kress G, Giger M, Ermanni P (2008) Complex shaped beam element and graph-based optimization of compliant mechanisms. Struct. Multidisc. Optim. 36:429–442

Sigmund O (2001) A 99 line topology optimization code written in Matlab. Struct. Multidisc. Optim. 21(2):120–127

Sigmund O (2007) Morphology-based black and white filters for topology optimization. Struct Multidisc Opt 33:401–424

Sigmund O, Maute K (2013) Topology optimization approaches: a comparative review. Struct. Multidisc. Opt. 48(6):1031–1055

Sigmund O, Peterson J (1998) Numerical instabilities in topology optimization: a survey on procedures dealing with checkerboards. Mesh dependencies and local minima. Struct. Optim. 16:68–75

Sobieski SJ, Haftka RT (1997) Multidisciplinary aerospace design optimization: survey of recent developments. Struct Optim 14:1–23

Stolpe M, Svanberg K (2001a) An alternative interpolation scheme for minimum compliance topology optimization. Struct Multidisc Optim 22:116–124

Svanberg K (1987) The method of moving asymptotes - a new method for structural optimization. Int J Numer Methods Eng 24:359–373

Tang MY (2014) Trust region algorithm with two sub-problems for bound constrained problems. Applied Math and Comput 242:778–789

Wang MY, Wang S (2005) Bilateral filtering for structural topology optimization. Int J Numer Methods Eng 63:1911–1938

Werme M (2008) Using the sequential linear integer programming method as a post-processor for stress-constrained topology optimization problems. Int J Numer Methods Eng 76:1544–1567

Wood DW, Groenwold AA (2010) On concave constraint functions and duality in predominantly black-and-white topology optimization. Comput Methods Appl Mech Eng 199:2224–2234

Xia L, Zhu JH, Zhang WH (2012) Sensitivity analysis with the modified Heaviside function for the optimal layout design of multi-component systems. Comput Methods Appl Mech Engrg 241–244:142–154

Yin L, Yang W (2001) Optimality criteria method for topology optimization under multiple constraints. Comput Struct 79:1839–1850

Zhou M, Rozvany GIN (1991) The COC algorithm, part II: topological, geometry and generalized shape optimization. Comput Methods Appl Mech Eng 89:197–224

Zuo ZH, Xie YM (2014) Evolutionary topology optimization of continuum structures with a global displacement control. Comput Aided Des 56:58–67

Zuo ZH, Xie YM, Huang X (2012) Evolutionary topology optimization of structures with multiple displacement and frequency constraints. Adv Struct Eng 15(2):385–398